Biophysical Journal, Volume 99

Supporting material

Synergy between CaMKII substrates and β-adrenergic signaling in regulation of cardiac myocyte Ca^{2+} handling

Anthony R. Soltis and Jeffrey J. Saucerman

SUPPLEMENTARY MATERIALS
SYNERGY BETWEEN CAMKII SUBSTRATES AND β-ADRENERGIC SIGNALING IN REGULATION OF CARDIAC MYOCYTE Ca^{2+} HANDLING

Soltis, A.R. and Saucerman J.J.

Target	Kinase	Dynamic Regulation	Description
LCC	CaMKII/PKA	Yes/Yes	Enhanced I_{Ca} opening probability (both), facilitation (CaMKII), and recovery from inactivation (CaMKII), via phosphorylation-dependent increases in fraction of mode 2 gating. PKA also increases fraction of available channels.
RyR	CaMKII/PKA	Yes/Yes	Enhanced channel opening probability (both) and leak (CaMKII) due to channel phosphorylation.
PLB	CaMKII/PKA	Yes/Yes	Enhanced Ca^{2+}-sensitivity of SERCA pump (reduction of forward mode K_M) due to PLB phosphorylation (both kinases).
$I_{Na,f}$, $I_{Na,L}$	CaMKII	No	Shifted I_{Na} availability towards hyperpolarized potentials, delayed recovery from inactivation, and enhanced $I_{Na,L}$ magnitude.
I_{to}	CaMKII	No	Enhanced I_{to} magnitude (via $I_{to,s}$) and recovery from inactivation.
I_{Ks}	PKA	Yes	Enhanced channel availability and left-shifted current-voltage relationship
I_{CFTR}	PKA	Yes	Graded activation of current as a result of PKA phosphorylation
TnI	PKA	Yes	Decreased TnC affinity for Ca^{2+}

TABLE S1. Summary of Included Functional ECC Regulation Modules.

Parameter Name	Value	Units	Description	Source
V_{cyt}	2.14×10^{-11}	L	Cytosolic volume	(5)*
V_{dyad}	1.79×10^{-14}	L	Dyadic cleft volume	(5)*
$LCC_{tot\text{-}dyad}$	28.3	μM	Total dyadic [LCC] (μmol/L dyad)	(8-9)†
$LCC_{tot\text{-}sl}$	84.6	nM	Total subsarcolemmal [LCC] (nmol/L sl)	(8-9)†
$RyR_{tot\text{-}dyad}$	382.6	μM	Total dyadic [RyR]	(8-9)†
PLB_{tot}	38	μM	Total cytosolic [PLB]	(8, 10)†
$PP1$	95.6	μM	Total dyadic [PP1]	(11)‡
$PP2A$	95.6	μM	Total dyadic [PP2A]	(11)‡
$CaMKII_{tot}$	120	μM	Total dyadic [CaMKII]	(12)*
k_{CK_LCC}	0.4	1/s	CaMKII phosphorylation rate at LCC	(13-14)†, (1, 15)‡
$k_{PP1\text{-}LCC}$	0.1103	1/s	PP1 dephosphorylation rate at LCC	(16-17)†, (1, 15)‡

$K_{M\_CK\text{-}LCC}$	12	μM	Michaelis Constant for CaMKII phosphorylation at LCC	(13)*, (14)‡
$K_{M\_PP1\text{-}LCC}$	9	μM	Michaelis Constant for PP1 dephosphorylation at LCC	(17)*, (16)‡
k_{b_2815}	0.35	1/s	Basal phosphorylation of Ser^{2815}	(18)§
k_{CK_RyR}	0.4	1/s	CaMKII phosphorylation rate at RyR	(16-17)†, (15)‡
k_{PP1_RyR}	1.07	1/s	PP1 dephosphorylation rate at RyR	(16-17)†
k_{PP2A_RyR}	0.481	1/s	PP2A dephosphorylation rate at RyR	(16-17, 19)†‡, (18)§
$K_{M\_CK\text{-}RyR}$	12	μM	Michaelis Constant for CaMKII phosphorylation at RyR	(13)*, (14)‡
$K_{M\_PP1\text{-}RyR}$	9	μM	Michaelis Constant for PP1 dephosphorylation at RyR	(17)*, (16)‡
$K_{M\_PP2A\text{-}RyR}$	47	μM	Michaelis Constant for PP2A dephosphorylation at RyR	(17)*, (16)‡
k_{CK_PLB}	0.008	1/s	CaMKII phosphorylation rate at PLB	(16-17)†, (15)‡
k_{PP1_PLB}	0.0428	1/s	PP1 dephosphorylation rate at PLB	(16-17)†
$K_{M\_CK\text{-}PLB}$	12	μM	Michaelis constant for CaMKII phosphorylation at PLB	(13)*, (14)‡
$K_{M\_PP1\text{-}PLB}$	9	μM	Michaelis constant for PLB dephosphorylation at PLB	(17)*, (16)‡
$K_{i\_OA\text{-}PP1}$	780	nM	Inhibitory constant of OA on PP1	(18)§‡
$K_{i\_OA\text{-}PP2A}$	37	nM	Inhibitory constant of OA on PP2a	(18)§‡

TABLE S2. CaMKII phosphorylation parameters. Parameters are direct (*), derived (†), or estimated/assumed (‡) from experimental sources. Parameters denoted with '§' were determined through parameter estimation against data from cited sources.

Parameter	*Value*	*Description*	*Units*
Lig_{tot}	Variable (0-1.0)	Total ligand (ISO) concentration	μM
$LCC_{tot\text{-}BA}$	0.025	Total [LCC] per liter cytosol	μM
$RyR_{tot\text{-}BA}$	0.135	Total [RyR] per liter cytosol	μM
$PLB_{tot\text{-}BA}$	38	Total [PLB] per liter cytosol	μM
$TnI_{tot\text{-}BA}$	70	Total [TnI] per liter cytosol	μM
$IKs_{tot\text{-}BA}$	0.025	Total [I_{Ks}] channels per liter cytosol	μM
$CFTR_{tot\text{-}BA}$	0.025	Total [CFTR] channels per liter cytosol	μM
$PP1_{PLB\text{-}tot\text{-}BA}$	0.89	Total [PP1] in the vicinity of PLB per liter cytosol	μM

TABLE S3. Total Protein Concentrations in β-AR model. Total PKA target concentrations as assigned in Saucerman et al. (2004) (20). A full list of parameter values can be found in the previous publication.

Figure	Simulation Protocols
1	None.
2	(**A**) Steady state pacing at 0.5 Hz during CaMKII OE with abrupt switch to 2.0 Hz pacing at 4 s time point in figure. (**B-D**) Average, steady state phosphorylation levels at labeled targets.
3	(**A**) 1 Hz paced, steady state $[Ca^{2+}]_i$ transients. (**B**) AP traces during same conditions in **A**. (**C-D**) 1 Hz, steady state values for each parameter explained in legend. (**E-F**) Steady state values of each parameter at various frequencies under listed conditions.
4	(**A**) Model was stimulated to 0.25 Hz steady state and abruptly switched to 1 Hz pacing. (**B**) Model stimulated to steady state at 2 Hz voltage clamp (-80 mV holding potential, 0 mV test, 200 ms pulse duration).
5	(**A**) Steady state, 2 Hz dyadic CaMKII transients for each condition. (**B-C**) Steady state values were taken with some target phosphor-regulation fixed at control levels. (**D**) Steady state 2 Hz $[Ca^{2+}]_i$ transients for listed conditions.
6	Protocol discussed in text, figure, and figure legend.
S1	(**B-C**) Protocol labeled in figure (and described below for Fig. S2).
S2	(**A**) 2.0 Hz voltage clamp from -90 mV holding potential to -50 mV for 50 ms then to 0 mV test potential for 200 ms (at 295ºK, see inset in Fig S1 *B*). Protocol begun from -90 mV rest. (**B**) Experimental data from (1).
S3	(**A**) Same protocol as shown in Fig S1 (0.5 Hz). (**B**) For each test potential, 0.5 Hz voltage clamp (protocol in S1) was applied until steady was reached; reported values are peak I_{Ca} minus residual. (**C**) For all conditions, 1 Hz voltage clamp from -70 mV to 0 mV test potential for 10 s (to activate CaMKII), 2 s rest at -90 mV, 500 ms square pulse to 0 mV, rest at -90 mV for variable length of time, followed by additional 500 ms pulse to 0 mV. All simulations were performed at 295ºK. (**D-F**) Experimental data from (1).
S4	Model run at various [OA] until steady state Ser^{2815} phosphorylation achieved; values normalized to phosphorylation level at saturating [OA].
S5	Steady state phosphorylation at RyR for labeled condition.
S6	2 Hz steady state PLB phosphorylation level with and without inclusion of inhibitor-1/PP1 interaction.
S7	(**A**) 500 ms voltage clamp to -20 mV from -140 mV holding potential. (**B**) Steady-state $[Na]_i$ levels predicted by model. (**C**) Experimental data from (6).
S8	(**A**) 500 ms square pulse to 50 mV from -80 mV, followed by hold at -80 mV for variable length of time and an additional 500 ms pulse to 50 mV. Data points from (2) (**B**) 1 Hz I_{to} during pacing.
S9	1 Hz pacing during labeled test conditions.

S10	1 Hz pacing to steady state, 30 s rest, and additional paced beat.
S11	Steady state pacing t_{50}s for $\Delta[Ca^{2+}]_i$ at indicated frequencies.
S12	Pacing protocol described in figure legend and listed above panels **A** and **B**.
S13	1 Hz pacing with 1 μM ISO for 60s.
S14	Protocol described in figure legend.
S15	Protocol described in figure legend.

Table S4. Simulation protocols for individual figures.

CAMKII AND PKA PHOSPHORYLATION MODULES

Non-competitive Okadaic Acid inhibition terms (x = 1 or 2A)

$$OA_{PPx} = 1/\left(1 + \left([OA]/K_{i_{OA-PPx}}\right)^3\right)$$

LCC MODULE

L-type calcium channels (LCCs) are responsible for the majority of Ca^{2+} influx during systole (21). In rabbit myocytes, total [LCC] is ~26.3 nmol/L cytosol (8-9); assuming 90% dyadic and 10% subsarcolemmal placement (as in the Shannon model (5)), total [LCC] was set to 28.3 μM and 84.6 nM in the dyad and subsarcolemma, respectively. CaMKII can phosphorylate LCCs at a number of sites, including Ser^{1512} and Ser^{1570} on the α subunit (22-23) and Thr^{498} on the β_{2a} subunit (24). No specific distinction is made between sites in the model for simplicity and PP1 is assumed to be the main phosphatase that opposes CaMKII phosphorylation (25-26). We assume that dyadic cleft channels are regulated by dyadic cleft CaMKII. Similarly, subsarcolemmal channels are only regulated by subsarcolemmal CaMKII.

Numerous studies have demonstrated that CaMKII is necessary for LCC current (I_{Ca}) facilitation, the phenomenon of positive staircase in macroscopic I_{Ca} amplitude after repetitive depolarization from rest (Fig. S2) (7, 23-24, 27-29). As the time course of facilitation is fast (completes within 5-10 pulses), CaMKII-LCC phosphorylation kinetics were assumed to be quick (as suggested by Huke and Bers (15)). Experimental (27) and modeling (30) studies demonstrated that facilitation is the result of a CaMKII-induced shift in the distribution of LCC gating modes. Namely, CaMKII increases the fraction of LCCs gating in mode 2, a mode characterized by long channel openings (in contrast to mode 1 gating which is characterized by frequent, short openings) (27).

To model the effect of CaMKII phosphorylation on modal gating, we replaced the existing ECC model's LCC model with the seven-state Markovian scheme developed by Mahajan et al. (31) (Fig. S1 *A*). Parameter adjustments were made during implementation to preserve the Ca^{2+}-handling characteristics of the original ECC model and to match relevant experimental readouts, including I_{Ca} amplitude ($G_{Ica\text{-}current}$), Ca^{2+}-inactivation (*cp-bar,* and k_o^p) and recovery from inactivation (k_5 and k_{5p}). Four sets of changes to Markov state transitions were implemented in the ECC model: two for mode 1 dyadic cleft and subsarcolemmal channels and an additional two for mode 2 channels in each compartment. In keeping with previous representations of mode 2 gating (30, 32), the voltage-independent rate constant r_2 was reduced from 3.0 to 0.3 ms for mode 2 channels. This alteration resulted in an increase in peak channel opening probability during 0 mV voltage clamp from ~0.05 to ~0.25 (consistent with mean LCC opening probability data from Dzhura et al. (27)) (Fig. S1 *B*) and a reduction in the rate of channel inactivation (Fig. S1 *C*). It is important to note that the values of parameters s_2 and s_2' (or s_{2p}) are dependent on the value of r_2 through the principle of microscopic reversibility (31). Therefore, these parameters were redefined in cases where r_2 was altered to preserve these constraints. Total I_{Ca} is the sum of all currents from mode 1 and mode 2 channels.

We assume that with no CaMKII or PKA phosphorylation, all LCCs gate in mode 1. CaMKII phosphorylation increases the distribution of mode 2 channels, though this effect is appreciable only in the dyadic cleft (where CaMKII signals are strongest). We do not assume a 1:1 relationship between phosphorylation and number of mode 2 channels; rather, CaMKII is assumed to, at most, shift 10% of channels to mode 2 (as in data from highly phosphorylated

single channel studies (27, 33)). This effect was implemented with a simple linear function of fractional LCC phosphorylaton that enhances the percentage of channels obeying mode 2 parameters (see below equations).

Our new CaMKII-LCC model was able to reproduce a number of typical experimental readouts for CaMKII-dependent regulation of I_{Ca}. As shown Fig. S2, the model displays CaMKII-dependent I_{Ca} facilitation that is enhanced with CaMKII overexpression and reversed during rapid (2 Hz) pacing with CaMKII inhibition. Fig S3 *A* shows sample I_{Ca} traces at 0.5 Hz voltage clamp where peak current was increased from -5.6 to -6.7 A/F with CaMKII overexpression (similar to experimental data in Fig. S3 *D*). The overall current-voltage (I-V) relationship of I_{Ca} (Fig. S3 *B*) is consistent with experimental data (Fig. S3 *E*), where CaMKII overexpression increased current magnitude without altering the voltage dependence of I_{Ca}. Also, our model displays CaMKII-dependent hastening of LCC recovery from inactivation (Fig S3 *C* model**,** Fig. S3 *F* data).

PKA also phosphorylates the α_{1C} and β_{2a} subunits of LCCs with distinct functional consequences. As we have modeled previously (20), phosphorylation at α_{1C} sites increases channel opening probability while β_{2a} phosphorylation increases channel availability. Adrenergic stimulation has also been shown to enhance the proportion of channels gating in mode 2 (33). We implemented PKA-dependent shifting of channels to mode 2 as a function of α_{1C} phosphorylation assuming that, at most, PKA shifts 15% of all channels to mode 2 (similar to values assumed in (32)). PKA percentage phosphorylation of dyadic cleft and subsarcolemmal LCCs is assumed to be equal, given our previous assumption of equivalent PKA activation in both compartments. Lastly, the effects of PKA-dependent β_{2a} subunit phosphorylation were implemented by multiplying all LCC currents by a factor f_{avail}, which is an increasing linear function of β_{2a}-phosphorylated channels.

CaMKII-dependent LCC Phosphorylation equations (see Saucerman et al. (2004) (20) for PKA phosphorylation reactions)

$$[LCC_{CKn}] = [LCC_{Tot-x}] - [LCC_{CKp}]$$

$$Rxn_{CK-LCC} = \frac{k_{CK\_LCC}[CaMKII_{act}][LCC_{CKn}]}{K_{M_{CK-LCC}} + [LCC_{CKn}]}$$

$$Rxn_{PP1-LCC} = \left(\frac{k_{PP1\_LCC}[PP1][LCC_{CKp}]}{K_{M_{PP1-LCC}} + [LCC_{CKp}]}\right) OA_{PP1}$$

$$\frac{d[LCC_{CKp}]}{dt} = Rxn_{CK-LCC} - Rxn_{PP1-LCC}$$

L-Type Calcium Channel (LCC) Markov Model

Fixed Parameters/Transition Rates

Parameter Name	**Value**	**Units**
pCa	5.4×10^{-4}	cm/s

τ_{po}	1	ms
T_{Ba}	450	ms
s_{1o}	0.0221	1/ms
k_{1o}	0.03	1/ms
k_o^p*	2.5	μM
$\overline{cp}$ *or cp-bar**	8.0	μM
r_1	0.3	1/ms
r_2	3.0 (mode 1), 0.3 (mode 2)	1/ms
s_{1p}	0.00195	1/ms
k_{1p}	0.00413	1/ms
k_2	1 x 10^{-4}	1/ms
k_{2p}	0.00224	1/ms
$G_{Ica\text{-}current}$*	5.25	1/cm/L/F
$F_{junc\text{-}CaL}$†	0.9	None
$F_{sl\text{-}CaL}$†	0.1	None
$Q_{10\text{-}CaL}$†	1.8	None
pK†	2.7 x 10^{-7}	cm/s
pNa†	1.5 x 10^{-8}	cm/s

* Indicate parameters that differ from original Mahajan et al. model (31).
† Indicates parameters taken from original LCC model in Shannon et al. (5).

Voltage and Ca-dependent parameters:
Note – Ca_x represents a Ca concentration in either the dyadic cleft ('j') or subsarcolemma ('sl').

$$p_o^{\infty} = 1/\left(1 + e^{-\frac{V}{8}}\right)$$

$$f(Ca_x) = 1/\left(1 + \left(\frac{k_p^o}{Ca_x}\right)^3\right)$$

$$R(V) = 10 + 4954e^{V/15.6}$$

$$\Pr = 1 - 1/\left(1 + e^{-\frac{(V+40)}{4}}\right)$$

$$Ps = 1/\left(1 + e^{-\frac{(V+40)}{11.32}}\right)$$

$$T_{Ca} = \frac{78.0329 + 0.1\left(1 + \left(\frac{Ca_x}{\overline{cp}}\right)^2\right)}{1 + \left(\frac{Ca_x}{\overline{cp}}\right)^2}$$

$$\tau_{Cax} = (R(V) - T_{Ca})Pr + T_{Ca}$$

$$\tau_{Ba} = (R(V) - T_{Ba})Pr + T_{Ba}$$

Transitions Rates:

$$\alpha = p_o^{\infty}/\tau_{po}$$

$$\beta = (1 - p_o^{\infty})/\tau_{po}$$

$$s_1 = s_{1o} f(Ca_x)$$

$$k_1 = k_{1o} f(Ca_x)$$

$$s_2 = s_1 \left(\frac{k_2}{k_1}\right)\left(\frac{r_1}{r_2}\right)$$

$$s_{2p} = s_{1p} \left(\frac{k_{2p}}{k_{1p}}\right)\left(\frac{r_1}{r_2}\right)$$

$$k_3 = \frac{e^{-(V+40)/3}}{3\left(1 + e^{\frac{-(V+40)}{3}}\right)}$$

$$k_{3p} = k_3$$

$$k_5 = (1 - Ps)/\,(3\tau_{Cax})$$

$$k_6 = f(Ca_x)Ps/\,\tau_{Cax}$$

$$k_{5p} = (1 - Ps)/\,(3\tau_{Ba})$$

$$k_{6p} = Ps/\,\tau_{Ba}$$

$$k_4 = k_3 \left(\frac{\alpha}{\beta}\right)\left(\frac{k_1}{k_2}\right)\left(\frac{k_5}{k_6}\right)$$

$$k_{4p} = k_{3p} \left(\frac{\alpha}{\beta}\right)\left(\frac{k_{1p}}{k_{2p}}\right)\left(\frac{k_{5p}}{k_{6p}}\right)$$

Differential Equations for Markov States

$$P_o = 1 - (C_1 + C_2 + I_{1Ca} + I_{2Ca} + I_{1Ba} + I_{2Ba})$$

$$\frac{dC_2}{dt} = \beta C_1 + k_5 I_{2Ca} + k_{5p} I_{\boldsymbol{2Ba}} - (k_6 + k_{6p} + \alpha) C_2$$

$$\frac{dC_1}{dt} = \alpha C_2 + k_2 I_{1Ca} + k_{2p} I_{\mathbf{1Ba}} + r_2 P_{\boldsymbol{o}} - (r_1 + k_1 + \beta + k_{1p}) C_1$$

$$\frac{dI_{1Ca}}{dt} = k_1 C_1 + k_4 I_{2Ca} + s_1 P_{\boldsymbol{o}} - (k_2 + k_3 + s_2) I_{1Ca}$$

$$\frac{dI_{2Ca}}{dt} = k_3 I_{1Ca} + k_6 C_{\mathbf{2}} - (k_4 + k_5) I_{2Ca}$$

$$\frac{dI_{1Ba}}{dt} = k_{1p} C_1 + k_{4p} I_{2Ba} + s_{1p} P_{\boldsymbol{o}} - (k_{2p} + k_{3p} + s_{2p}) I_{1Ba}$$

$$\frac{dI_{2Ba}}{dt} = k_{3p} I_{1Ba} + k_{6p} C_{\mathbf{2}} - (k_{4p} + k_{5p}) I_{2Ba}$$

Where all Markov states are possible in mode 1 junctional (m1j), mode 2 junctional (m2j), subsarcolemmal mode 1 (slm1), or subsarcolemmal mode 2 (slm2) channels.

CaMKII- and PKA-dependent alterations to I_{Ca} and overall current equations

$$CKII_{m2x} = 0.1\left(\frac{[LCC_{CKp}]}{[LCC_{tot-x}]}\right)$$

$$PKA_{m2} = 0.1543\left(\frac{[LCC_{PKA-\alpha 1Cp}]}{[LCC_{tot-BA}]}\right) - 0.0043$$

$$frac_{LCC\beta po} = 0.0328$$

$$f_{avail} = 0.017\left(\frac{[LCC_{PKA-\beta p}]}{frac_{LCC\beta po}}\right) + 0.983$$

$$i_{Ca} = 4pCa\frac{VF^2}{RT}\frac{.001e^{\frac{2VF}{RT}} - 0.341[Ca]_o}{e^{\frac{2VF}{RT}} - 1}$$

$$Q_{pow} = (T - 310)/10$$

$$I_{Caj-m1} = F_{junc-CaL}\left(G_{ICa-current} i_{Ca} P_{o-m1j}\right) Q_{10-CaL}^{Q_{pow}}$$

$$I_{Caj-m2} = F_{junc-CaL}\left(G_{ICa-current} i_{Ca} P_{o-m2j}\right) Q_{10-CaL}^{Q_{pow}}$$

$$junc_{m2} = CKII_{m2junc} + PKA_{m2}$$

$$I_{Caj} = (1 - junc_{m2}) I_{Caj-m1} + (junc_{m2}) I_{Caj-m2}$$

$$I_{Casl-m1} = F_{sl-CaL}(G_{ICa-current} i_{Ca} P_{o-slm1}) Q_{10-CaL}^{Q_{pow}}$$

$$I_{Casl-m2} = F_{sl-CaL}(G_{ICa-current} i_{Ca} P_{o-slm2}) Q_{10-CaL}^{Q_{pow}}$$

$$sl_{m2} = CKII_{m2sl} + PKA_{m2}$$

$$I_{Casl} = (1 - sl_{m2}) I_{Caj-m1} + (sl_{m2}) I_{Caj-m2}$$

Potassium and Sodium currents through LCCs

$$i_{Ca-K} = pK \frac{VF^2}{RT} \frac{0.75[K]_i e^{\frac{2VF}{RT}} - 0.75[K]_o}{e^{\frac{2VF}{RT}} - 1}$$

$$I_{CaKj} = F_{junc-CaL} G_{ICa-current} i_{Ca-K} \left((1 - junc_{m2}) P_{o-m1j} + junc_{m2} P_{o-m2j}\right) Q_{10-CaL}^{Q_{pow}}$$

$$I_{CaKsl} = F_{sl-CaL} G_{ICa-current} i_{Ca-K} \left((1 - sl_{m2}) P_{o-m1j} + sl_{m2} P_{o-m2j}\right) Q_{10-CaL}^{Q_{pow}}$$

$$i_{Ca-Naj} = pNa \frac{VF^2}{RT} \frac{0.75[Na]_j e^{\frac{2VF}{RT}} - 0.75[Na]_o}{e^{\frac{2VF}{RT}} - 1}$$

$$i_{Ca-Nasl} = pNa \frac{VF^2}{RT} \frac{0.75[Na]_{sl} e^{\frac{2VF}{RT}} - 0.75[Na]_o}{e^{\frac{2VF}{RT}} - 1}$$

$$I_{CaNaj} = F_{junc-CaL} G_{ICa-current} i_{Ca-Naj} \left((1 - junc_{m2}) P_{o-m1j} + junc_{m2} P_{o-m2j}\right) Q_{10-CaL}^{Q_{pow}}$$

$$I_{CaNasl} = F_{sl-CaL} G_{ICa-current} i_{Ca-Na} \left((1 - sl_{m2}) P_{o-m1j} + sl_{m2} P_{o-m2j}\right) Q_{10-CaL}^{Q_{pow}}$$

Total LCC currents

$$I_{Ca} = I_{Caj} + I_{Casl}$$

$$I_{Ca-K} = I_{CaKj} + I_{CaKsl}$$

$$I_{Ca-Na} = I_{CaNaj} + I_{CaNasl}$$

$$I_{Ca-tot} = f_{avail}[I_{Ca} + I_{Ca-K} + I_{Ca-Na}]$$

RyR MODULE

RyRs are homotetrameric structures that control Ca^{2+} release from the SR during systole (8). Release is triggered by local dyadic cleft Ca^{2+} signals (Ca^{2+}-induced Ca^{2+} release) and the sensitivity of RyRs for Ca^{2+} is enhanced by CaMKII and PKA-dependent phosphorylation (34). [RyR] is estimated to be ~0.32 μmol monomer/L cytosol in rabbit ventricular myocytes (8-9). Assuming all RyRs reside in the dyadic cleft, total model [RyR] was set to 382.6 μmol/L dyad. [PP1] and [PP2A] were both set to 95.6 μM based on the assumption of 1 phosphatase molecule per RyR tetramer (11).

Several sites (Ser^{2809}, Ser^{2815}, and Ser^{2031} in rabbit) have been identified as targets for CaMKII or PKA-dependent RyR phosphorylation (15, 18, 34-38), though Ser^{2815} appears to be the main CaMKII target (1, 15, 18, 34). Huke and Bers (15) demonstrated that ~15% of Ser^{2815} sites are phosphorylated under basal conditions and that these levels are not dependent on CaMKII activity (18). To account for this, a CaMKII-independent basal phosphorylation rate was modeled as a first-order process against opposing PP1/PP2A dephosphorylation. The basal rate constant (k_b) was determined through parameter estimation (nonlinear least squares fitting in Matlab) with experimental data of increasing phosphatase inhibitor okadaic acid (OA) (Fig. S4) (18). Note that OA is a selective phosphatase inhibitor that blocks PP2A at low concentrations (IC_{50} of 2 nM) and PP1 at higher concentrations (IC_{50} of 270 nM) (16, 18). At 2 Hz pacing, CaMKII activity increases Ser^{2815} phosphorylation to ~25% (15), thus the catalytic rate constant for CaMKII phosphorylation was tuned to mimic this quantitative increase at the same frequency (Fig. 2 *C*, main text).

CaMKII phosphorylation has been shown to increase RyR opening probability (as demonstrated in lipid bilayers (34)) and SR leakage (1, 3, 38-41). While some groups have reported negative regulation of RyR opening (42) and suppression of Ca^{2+} sparks (a measure of spontaneous Ca^{2+} release through RyRs) (43) by CaMKII, a number of experiments in which SR content was tightly controlled strongly support positive CaMKII-dependent channel regulation (7, 39-40, 44). CaMKII overexpression in mouse (3, 41) and rabbit myocytes (1) showed enhancement of Ca^{2+} spark frequency, reduced $[Ca]_{SRT}$, and enhanced CaMKII-dependent RyR phosphorylation. Inhibition of CaMKII in rabbit myocytes increased $[Ca]_{SRT}$ (for a given SR leak) and decreased SR leak (for a given $[Ca]_{SRT}$) (39-40). Also, targeted CaMKII inhibition at the SR membrane in mouse myocytes resulted in decreased SR Ca^{2+} leakage and Ser^{2815} phosphorylation (45).

To mimic these experimental findings, the rate constants controlling Ca^{2+}-dependent opening of the RyR (k_{oCa}) and SR leak (k_{leak}) were re-implemented as functions of CaMKII-dependent RyR phosphorylation. The alteration to the Ca^{2+}-dependent RyR opening constant k_{oCa} increases CaMKII-dependent RyR Ca^{2+} sensitivity, leading to enhanced opening probability (as observed in bilayer data (34)). The alteration to k_{leak} represents a basal RyR flux which is mechanistically linked to RyR openings during diastole (e.g. via Ca^{2+} sparks). The alterations to these two parameters were necessary to produce sufficient RyR Ca^{2+}-sensitivity and leak during CaMKII overexpression that decreased $[Ca^{2+}]_{SRT}$ and, more modestly in some cases, $\Delta[Ca^{2+}]_i$ (as in experiments (1, 3)). Also, total leak during CaMKII overexpression increased between ~1.8 and ~2.6 times (at 0.5 and 3 Hz, respectively) compared to control, which is consistent with estimates of ~3 times more leak during overexpression from spark data (41).

PKA-dependent RyR phosphorylation also enhances channel Ca^{2+}-sensitivity and opening probability (11, 34), though PKA does not appear to significantly influence RyR-dependent diastolic leakage in normal (40, 44, 46) and failing (44) myocytes. Therefore, we

implemented PKA-dependent regulation of RyR opening by further enhancing the rate constant k_{oCa} as a linear function of RyR phosphorylation.

RyR Ser^{2815} Phosphorylation Equations (see Saucerman et al. (2004) (20) for PKA phosphorylation reactions)

$$[RyR_{2815n}] = [RyR_{Tot-Dyad}] - [RyR_{2815p}]$$

$$Rxn_{basal} = k_{b\_2815}[RyR_{2815n}]$$

$$Rxn_{CK-RyR} = \frac{k_{CK\_RyR}[CaMKII_{act}][RyR_{2815n}]}{K_{M_{CK-RyR}} + [RyR_{2815n}]}$$

$$Rxn_{PP1-RyR} = \left(\frac{k_{PP1\_RyR}[PP1][RyR_{2815p}]}{K_{M_{PP1-RyR}} + [RyR_{2815p}]}\right) OA_{PP1}$$

$$Rxn_{PP2A-RyR} = \left(\frac{k_{PP2A\_RyR}[PP2A][RyR_{2815p}]}{K_{M_{PP2A-RyR}} + [RyR_{2815p}]}\right) OA_{PP2A}$$

$$\frac{d[RyR_{2815p}]}{dt} = Rxn_{basal} + Rxn_{CK-RyR} - Rxn_{PP1-RyR} - Rxn_{PP2A-RyR}$$

Alterations to RyR opening (by PKA and CaMKII) and leak (CaMKII)

Parameter Name	**Value**	**Units**
k_s	25	1/ms
k_{oCa}	10	1/mM^2/ms
k_{om}	0.06	1/ms
k_{iCa}	0.5	1/mM/ms
k_{im}	0.005	1/ms
$EC_{50\text{-}SR}$	0.45	mM
Max_{SR}	15	None
Min_{SR}	1	None
H_{SR}	2.5	None
$k_{SR\text{-}leak}$	5.348 x 10^{-6}	1/ms

RyR gating. Parameters from Shannon et al. (5, 47) describing RyR opening transitions and leak.

$$\Delta k_{oRyR-CKII} = \frac{20}{3}\left(\frac{[RyR_{2815p}]}{[RyR_{Tot-Dyad}]}\right) - \frac{1}{3}$$

$$\Delta k_{oRyR-PKA} = 1.025\left(\frac{[RyR_{PKAp}]}{[RyR_{Tot-BA}]}\right) + 0.975$$

$$\Delta k_{oRyR} = \Delta k_{oRyR-CKII} + \Delta k_{oRyR-PKA} - 1$$

$$\Delta k_{leak} = \frac{1}{3} + \frac{10}{3}\left(\frac{[RyR_{2815p}]}{[RyR_{Tot}]}\right)$$

RyR Model

$$k_{CaSR} = Max_{SR} - \frac{Max_{SR} - Min_{SR}}{1 + \left(\frac{EC_{50-SR}}{[Ca]_{SR}}\right)^{H_{SR}}}$$

$$k_{oSRCa} = \Delta k_{oRyR}\left(\frac{k_{oCa}}{k_{CaSR}}\right)$$

$$k_{iSRCa} = k_{iCa}k_{CaSR}$$

$$RI = 1 - R - O - I$$

$$\frac{dR}{dt} = \left(k_{im}RI - k_{iSRCa}[Ca]_j R\right) - \left(k_{oSRCa}[Ca]_j^2 R - k_{om}O\right)$$

$$\frac{dO}{dt} = \left(k_{oSRCa}[Ca]_j^2 R - k_{om}O\right) - \left(k_{iSRCa}[Ca]_j O - k_{im}I\right)$$

$$\frac{dI}{dt} = \left(k_{iSRCa}[Ca]_j O - k_{im}I\right) - \left(k_{om}I - k_{oSRCa}[Ca]_j^2 RI\right)$$

$$J_{SRCaRel} = k_s O\left([Ca]_{SR} - [Ca]_j\right)$$

$$J_{SRLeak} = \Delta k_{leak}k_{SR-leak}\left([Ca]_{SR} - [Ca]_j\right)$$

PLB MODULE

PLB is a homopentameric protein that resides in the SR membrane and negatively regulates the SERCA pump. Phosphorylation relieves this inhibitory action and SERCA is allowed to more freely pump Ca^{2+} back into the SR during diastole (48). In ventricular myocytes, two PLB monomers exist per single SERCA molecule (8, 49). [SERCA] in rabbit myocytes is ~19 μmol/L cytosol (8, 10), thus total [PLB] was set to 38 μM in the model. CaMKII can phosphorylate PLB at Thr^{17} in a frequency dependent manner that is distinct from the PKA site at Ser^{16} (50-51). This interaction results in an increase in the Ca^{2+} sensitivity of the SERCA pump (i.e. a lowering of the forward pump rate K_m) (48, 52-54). While some groups have reported a direct CaMKII-SERCA interaction (at Ser^{38}) that results in a larger pump V_{Max} (independent of CaMKII interactions with PLB) (55-56), these results have been contested and may be artifacts of the particular experimental protocols used (48, 53). Given this controversy, no direct CaMKII-SERCA interaction was included in our model.

Our model predicts very weak cytosolic CaMKII activity (~10^{-4}%) due to weak Ca^{2+} signals and low total CaM and CaMKII in this compartment (12). These results suggest that PLB may be regulated by CaMKII signals that are distinct from those of the bulk cytosol. Physically, translocation of active CaMKII from the dyad to PLB could occur, though such a process has not been shown experimentally. Given that the only sufficiently strong CaMKII signals in our model are in the dyadic cleft and that CaMKII indeed phosphorylates PLB in a frequency dependent manner (50), we decided to model CaMKII regulation of PLB using dyadic cleft signals. To account for the slow kinetics of PLB phosphorylation observed experimentally (15, 57), the k_{cat} of this reaction was set to a value fifty times smaller than those of the LCC and RyR reactions (8 vs. 400 ms). Also, Huke and Bers showed that Thr^{17} phosphorylation levels are quantitatively low (< 5% at 2 Hz pacing) under normal conditions (15). This is evident when Thr^{17} phosphorylation levels are compared during pacing with and without OA, a strong positive control for maximal phosphorylation. Indeed, our model predicts low Thr^{17} phosphorylation levels during control scenarios (Fig. 2 *D*, main text), consistent with these quantitative findings.

One avenue for crosstalk between the CaMKII and PKA pathways is through inhibitor-1 (I-1). I-1 is activated during adrenergic stimulation via PKA phosphorylation and inhibits protein phosphatase 1 in the vicinity of PLB (58-59). This pathway was already present in the β-adrenergic signaling cascade and was extended to CaMKII-PLB interactions here. Specifically, the fraction of available PP1 molecules near PLB in our CaMKII signaling module was reduced in proportion to the amount of PP1 inhibition predicted by the β-adrenergic network (see equations and Fig. S6 for results).

CaMKII and PKA actions on PLB are functionally similar, with each kinase capable of lowering SERCA forward mode K_m by ~1/2 at maximum (53). In studies where Thr^{17} is mutated to Ala, phosphorylation at Ser^{16} alone is sufficient for mediating full responses to β-adrenergic stimulation (60). Given the similarity of these interactions, the total functional effect on K_{mf} was set to the maximal effect exerted by either kinase, thus preventing unrealistic additive interactions between the two effects.

PLB Thr^{17} Phosphorylation Equations (see Saucerman et al. (2004) (20) for PKA phosphorylation reactions)

$$[PLB_{T17n}] = [PLB_{Tot}] - [PLB_{T17p}]$$

$$Rxn_{CK-PLB} = \frac{k_{CK\_PLB}[CaMKII_{act}][PLB_{T17n}]}{K_{M_{CK-PLB}} + [PLB_{T17n}]}$$

$$[PP1_{PLB}] = \frac{[PP1_{PLB-avail-BA}]}{[PP1_{PLB-tot-BA}]}[PP1]$$

Where $PP1_{PLB\text{-}avail\text{-}BA}$ is the amount of available PP1 near PLB predicted by the β-adrenergic signaling model

$$Rxn_{PP1-PLB} = \left(\frac{k_{PP1\_PLB}[PP1_{PLB}][PLB_{T17p}]}{K_{M_{PP1-PLB}} + [PLB_{T17p}]}\right) OA_{PP1}$$

$$\frac{d[PLB_{T17p}]}{dt} = Rxn_{CK-PLB} - Rxn_{PP1-PLB}$$

Alterations to SERCA flux and SERCA Model

Parameter Name	**Value**	**Units**
$V_{Max\text{-}SERCA}$	286	µmol/l cytosol/s
K_{mf}	0.246	µM
K_{mr}	1.7	mM
H_{SERCA}	1.787	None
$Q_{10\text{-}SERCA}$	2.6	None

$$\Delta k_{SERCA-CKII} = 1 - 0.5\left(\frac{[PLB_{T17p}]}{[PLB_{Tot}]}\right)$$

$$frac_{PLBS16po} = .9926$$

$$\Delta k_{SERCA-PKA} = \frac{3}{4}\left(\frac{([PLB_{tot}] - [PLB_{S16p}])/[PLB_{tot}]}{frac_{PLBS16po}}\right) + \frac{1}{4}$$

$$\Delta k_{SERCA} = \min\left(\Delta k_{SERCA-CKII}, \Delta k_{SERCA-PKA}\right)$$

$$J_{SERCA} = Q_{10-SERCA}\frac{V_{Max-SERCA}\left(\frac{[Ca]_i}{K_{mf}\Delta k_{SERCA}}\right)^{H_{SERCA}} - V_{Max-SERCA}\left(\frac{[Ca]_{SR}}{K_{mr}}\right)^{H_{SERCA}}}{1 + \left(\frac{[Ca]_i}{K_{mf}\Delta k_{SERCA}}\right)^{H_{SERCA}} + \left(\frac{[Ca]_{SR}}{K_{mr}}\right)^{H_{SERCA}}}$$

Fast and Late Sodium Currents ($I_{Na,f}$ and $I_{Na,L}$)

The fast sodium current ($I_{Na,f}$) is identical to the formulation described in Shannon et al. (2004) (5) with the important addition of the late component ($I_{Na,L}$). The $I_{Na,L}$ formulation used is essentially the same as that described in Hund and Rudy (2008) (61). CaMKII overexpression in rabbit myocytes shifts I_{Na} availability in the hyperpolarizing direction, delays recovery from inactivation, and enhances the magnitude of the late Na^+ current (6). Similar to Hund and Rudy (2008) (61), these effects were implemented by shifting the voltage dependence of inactivation gates to the left, slowing the forward rate of the recovery gate 'j', and increasing the conductance of the late current. These altered properties were only selected during CaMKII overexpression simulations as no dynamic regulation of I_{Na} was included in the model. The effect of CaMKII overexpression on the late current is shown in Fig. S7.

I_{Na} and $I_{Na,L}$ parameters

Parameter	***Value***	***Units***
G_{Na}	16	mS/µF
F_{juncNa}	0.11	None
F_{slNa}	0.89	None
$G_{Na,L}$	0.013	mS/µF

CaMKII overexpression-dependent alterations to $I_{Na,f}$ and $I_{Na,L}$

if CaMKIIOE

$\text{INa}_{\text{shift}} = 3.25$ mV

$\alpha\text{CaMKII} = 0.18$

$\Delta\text{Gbar}_{\text{Na,L}} = 2$

else

$\text{INa}_{\text{shift}} = 0$ mV

$\alpha\text{CaMKII} = 0$

$\Delta\text{Gbar}_{\text{Na,L}} = 0$

Equations for $I_{Na,f}$

$$E_{Najunc} = \frac{RT}{F}\ln\frac{[Na]_o}{[Na]_{junc}}$$

$$E_{Nasl} = \frac{RT}{F}\ln\frac{[Na]_o}{[Na]_{sl}}$$

$$\alpha_m = \frac{0.32(V+47.13)}{1-e^{-0.1(V+47.13)}} \qquad \beta_m = 0.08e^{-V/11}$$

if $V + \text{INa}_{\text{shift}} \geq -40$

$$\alpha_h = 0, \alpha_j = 0$$

$$\beta_h = \frac{1}{0.13\left(1+e^{\frac{-\left(V+10.66+INa_{shift}\right)}{11.1}}\right)}$$

$$\beta_j = \frac{0.3e^{(-2.535\ x\ 10^{-7}(V+INa_{shift})}}{1+e^{-0.1(V+32+INa_{shift})}}$$

else

$$\alpha_h = 0.135e^{-(V+80+INa_{shift})/6.8}$$

$$\alpha_j = (1-\alpha CaMKII)\frac{\left(-1.2714\ x\ 10^5 e^{0.2444(V+INa_{shift})} - 3.474\ x\ 10^{-5}e^{-0.04391(V+INa_{shift})}(V+37.78+INa_{shift})\right)}{1+e^{0.311(V+79.23+INa_{shift})}}$$

$$\beta_h = 3.56e^{0.079(V+INa_{shift})} + 3.1\ x\ 10^5 e^{0.35(V+INa_{shift})}$$

$$\beta_j = \frac{0.1212e^{-0.01052(V+INa_{shift})}}{1+e^{-0.1378(V+40.14+INa_{shift})}}$$

$$\frac{dm}{dt} = \alpha_m(1-m) - \beta_m m$$

$$\frac{dh}{dt} = \alpha_h(1-h) - \beta_h h$$

$$\frac{dj}{dt} = \alpha_j(1-j) - \beta_j j$$

$$I_{Na,junc} = F_{juncNa}G_{Na}m^3hj(V-E_{Najunc})$$

$$I_{Na,sl} = F_{slNa}G_{Na}m^3hj(V-E_{Nasl})$$

$$I_{Na,f} = I_{Na,junc} + I_{Na,sl}$$

Equations for $I_{Na,L}$

$$\overline{G_{Na,L}} = G_{Na,L}(1+\Delta Gbar_{Na,L})$$

$$\alpha_{m,L} = \frac{0.32(V+47.13)}{1-e^{-0.1(V+47.13)}} \qquad \beta_{m,L} = 0.08e^{-V/11}$$

$$\frac{dm_L}{dt} = \alpha_{m,L}(1-m_L) - \beta_{m,L}m_L$$

$$h_{L,\infty} = 1/\left(1+e^{(V+91)/6.1}\right)$$

$$\tau_{h,L} = 600 \text{ ms}$$

$$\frac{dh_L}{dt} = \frac{h_{L,\infty} - h_L}{\tau_{h,L}}$$

$$I_{Na,L,junc} = F_{juncNa}\overline{G_{Na,L}}m_L^3 h_L(V - E_{Najunc})$$

$$I_{Na,L,sl} = F_{slNa}\overline{G_{Na,L}}m_L^3 h_L(V - E_{Nasl})$$

$$I_{Na,L} = I_{Na,L,junc} + I_{Na,L,sl}$$

Total sodium current (I_{Na})

$$I_{Na} = I_{Na,f} + I_{Na,L}$$

Transient-outward Potassium Current (I_{to})

The I_{to} formulation ($I_{to,f}$ + $I_{to,s}$, fast plus slow components) is essentially the same as in Shannon et al. (2004) (5) with the adjustments described in Grandi et al. (2007) (62). Acute CaMKII overexpression in rabbit ventricular myocytes has been shown to increase I_{to} amplitude (via increased $I_{to,s}$) and recovery from inactivation (2). In these studies, protein expression for the channel forming subunit of $I_{to,s}$ ($K_v1.4$) is significantly increased, possibly the result of CaMKII-dependent transcriptional regulation. Given that the mechanisms underlying CaMKII-dependent regulation of I_{to} are somewhat unclear (2), these effects were implemented during CaMKII overexpression simulations only. As in Grandi et al. (2007) (62), $I_{to,s}$ conductance and gating was altered to mimic enhanced $I_{to,s}$ amplitude and recovery from inactivation (Fig. S8).

I_{to} Parameters

Parameter	***Value***	***Units***
$G_{to,f}$	0.02	mS/µF
$G_{to,s}$	0.06	mS/µF

CaMKII overexpression-dependent changes to I_{to}

if CaMKIIOE

$Py = 15$

$Pr1 = 3600$

$Pr2 = 500$

$\Delta G_{to,slow} = 1.5$

else

$Py = 182$

$Pr1 = 8085$

$Pr2 = 313$

$\Delta G_{to,slow} = 1$

Equations for $I_{to,s}$

$$E_K = \frac{RT}{F}\ln\frac{[K]_o}{[K]_i}$$

$$X_{to,s,\infty} = 1/\left(1 + e^{-(V+3)/15}\right)$$

$$Y_{to,s,\infty} = 1/\left(1 + e^{(V+33.5)/10}\right)$$

$$R_{to,s,\infty} = 1/\left(1 + e^{(V+33.5)/10}\right)$$

$$\tau_{Xto,s} = \left[9/\left(1 + e^{(V+3)/15}\right)\right] + 0.5$$

$$\tau_{Yto,s} = \left[Py/\left(1 + e^{(V+33.5)/10}\right)\right] + 1$$

$$\tau_{Rto,s} = \left[Pr1/\left(1 + e^{(V+33.5)/10}\right)\right] + Pr2$$

$$\frac{dX_{to,s}}{dt} = \frac{X_{to,s,\infty} - X_{to,s}}{\tau_{Xto,s}}$$

$$\frac{dY_{to,s}}{dt} = \frac{Y_{to,s,\infty} - Y_{to,s}}{\tau_{Yto,s}}$$

$$\frac{dR_{to,s}}{dt} = \frac{R_{to,s,\infty} - R_{to,s}}{\tau_{Rto,s}}$$

$$I_{to,s} = \Delta G_{to,slow} G_{to,s} X_{to,s} Y_{to,s} (V - E_k)$$

Equations for $I_{to,f}$

$$X_{to,f,\infty} = 1/\left(1 + e^{-(V+3)/15}\right)$$

$$Y_{to,f,\infty} = 1/\left(1 + e^{(V+33.5)/10}\right)$$

$$\tau_{Xto,f} = 3.5e^{-((V+3)/30)^2} + 1.5$$

$$\tau_{Yto,f} = \left[20/\left(1 + e^{(V+33.5)/10}\right)\right] + 20$$

$$\frac{dX_{to,f}}{dt} = \frac{X_{to,f,\infty} - X_{to,f}}{\tau_{Xto,f}}$$

$$\frac{dY_{to,f}}{dt} = \frac{Y_{to,f,\infty} - Y_{to,f}}{\tau_{Yto,f}}$$

$$I_{to,f} = G_{to,f} X_{to,f} Y_{to,f} (V - E_k)$$

Total I_{to}

$$I_{to} = I_{to,f} + I_{to,s}$$

Slow Delayed Rectifier Potassium Channel Current (I_{Ks})

The formulation for I_{Ks} is identical to that of Shannon et al. (2004) (5), though we included dynamic regulation of the current by PKA. When PKA is activated, the fraction of available I_{Ks} channels ($f_{IKs\text{-}avail}$) is increased and the current-voltage relationship is shifted leftward. These changes were implemented as linear functions of fractional channel phosphorylation by PKA (as in Saucerman et al. (2004) (20)).

Fixed I_{Ks} Parameters

Parameter	***Value***	***Units***
p_{NaK}	0.01833	mS/µF
$F_{xKs\text{-}junc}$	0.11	None
$F_{xKs\text{-}sl}$	0.89	None

PKA-dependent Regulation of I_{Ks}

$$frac_{IKspo} = 0.0720$$

$$frac_{IKsp} = IKs_p / IKs_{tot}$$

$$frac_{IKsavail} = 0.2(frac_{IKsp}/frac_{IKspo}) + 0.8$$

$$Xs_{05} = 1.5(2 - frac_{IKsp}/frac_{IKspo})$$

Equations for I_{Ks}

$$pCa_x = 3 - \log_{10} Ca_x$$

Where *x* represents either the junctional or sub-sarcolemmal compartment

$$\overline{G_{Ksx}} = frac_{IKsavail} 0.07 \left(0.057 \frac{0.19}{1 + e^{(-7.2 + pCa_x)/0.6}}\right)$$

$$E_{Ks} = \frac{RT}{F} \ln \frac{[K]_o + p_{NaK}[Na]_o}{[K]_i + p_{NaK}[Na]_x}$$

$$X_{s,\infty} = 1/\left(1 + e^{-(V - Xs_{05})/16.7}\right)$$

$$\tau_{xs} = \frac{1}{\frac{7.19\ x\ 10^{-5}(V+30)}{1 - e^{-0.148(V+30)}} + \frac{1.31\ x\ 10^{-4}(V+30)}{e^{0.0687(V+30)} - 1}}$$

$$\frac{dX_s}{dt} = \frac{X_{s,\infty} - X_s}{\tau_{xs}}$$

$$I_{Ksx} = F_{xKs-x}\,\overline{G_{Ksx}} X_s^2 (V - E_{Ks})$$

$$I_{Ks} = I_{Ks-junc} + I_{Ks-sl}$$

Cystic Fibrosis Transmembrane Conductance Regulator Current (I_{CFTR} or $I_{Cl(cAMP)}$)

β-adrenergic stimulation activates a time and E_m-independent outward chloride current in cardiac myocytes (63-64). This current is carried by the cardiac variant of the cystic fibrosis transmembrane conductance regulator (CFTR) whose sequence in rabbit myocytes shows >90% similarity to human epithelial cell CFTR (65). PKA appears to be tightly coupled to CFTR channels through AKAP-mediated targeting and I_{CFTR} magnitude is graded with respect to PKA activity levels (66). We added PKA-dependent phosphorylation and activation of CFTR channels to the β-adrenergic signaling module, assuming similar CFTR density as I_{Ks} channels. We assume a 1:1 ratio of PKA molecules to CFTR channels and, given the PKA-CFTR scaffold, that phosphorylation reactions are subject to scaling by a factor ε (set to 10 by default (67)) to increase the effective concentration of the substrate. In response to 10 μM Forskolin, CFTR phosphorylation reaches steady state in ~30 s, consistent with the experimentally measured time course for Forskolin-induced activation of I_{CFTR} (between 26 and 46 s) (66) (see Fig. S13 *B*, second row middle for phosphorylation kinetics). I_{CFTR} was modeled with the simple ohmic formulation used in Shannon et al. (2005) (47), though its conductance increases as a linear function of PKA-dependent phosphorylation.

CFTR Module Parameters

Parameter	***Value***	***Units***
$CFTR_{tot}$	0.025	μM
$PKAIIC_{CFTR\text{-}tot}$	0.025	μM
$PKAII_{tot}$	0.084	μM
$PP1_{CFTR}$	0.025	μM
$k_{PKA\text{-}CFTR}$	54	1/s
$K_{M\text{-}PKA\text{-}CFTR}$	8.5	μM
$k_{PP1\text{-}CFTR}$	8.52	1/s
$K_{M\text{-}PP1\text{-}CFTR}$	7	μM
ε	10	none
G_{CFTR}	4.9×10^{-3}	mS/μF

PKA-dependent phosphorylation of CFTR channels

$$[CFTR_n] = [CFTR_{tot}] - [CFTR_p]$$

$$[PKAIIC_{CFTR}] = [PKAIIC_{CFTR-tot}]\left(\frac{[PKAII_{act}]}{[PKAII_{tot}]}\right)$$

$$CFTR_{phos} = \frac{\varepsilon k_{PKA-CFTR}[PKAIIC_{CFTR}][CFTR_n]}{K_{M-PKA-CFTR} + \varepsilon[CFTR_n]}$$

$$CFTR_{dephos} = \frac{\varepsilon k_{PP1-CFTR}[PP1_{CFTR}][CFTR_p]}{K_{M-PP1-CFTR} + \varepsilon[CFTR_p]}$$

$$\frac{d[CFTR_p]}{dt} = CFTR_{phos} - CFTR_{dephos}$$

Equations for I_{CFTR}

$$E_{Cl} = \frac{RT}{F}\ln\frac{[Cl]_i}{[Cl]_o}$$

$$fact_{PKA-CFTR} = 1.1933\left(\frac{[CFTR_p]}{[CFTR_{tot}]}\right) - 0.1933$$

$$I_{CFTR} = fact_{PKA-CFTR}\, G_{CFTR}(V - E_{Cl})$$

TnI regulation by PKA

As in our previous β-adrenergic signaling model (20, 68), PKA phosphorylation of troponin I (TnI) decreases myofilament Ca^{2+} sensitivity by increasing the K_d of TnC for Ca^{2+}. The phosphorylation and regulatory equations were taken directly from our previous models and implemented in the Shannon ECC model.

TnC parameters

Parameter	***Value***	***Units***
$B_{max\text{-}TnCl}$	70	μM
$k_{off\text{-}TnCl}$	19.6 x 10^{-3}	1/ms
$k_{on\text{-}TnCl}$	32.7	1/mM/ms

Regulation of TnC Ca^{2+} affinity

$$frac_{TnIpo} = .0031$$

$$f_{PKA-TnI} = \left(1.45 - 0.45\left(\frac{1 - TnI_p/TnI_{tot-BA}}{1 - frac_{TnIpo}}\right)\right)$$

$$\frac{d[TnCl:Ca]}{dt} = k_{on-TnCl}[Ca]_i([B_{max-TnCl}] - [TnCl:Ca]) - f_{PKA-TnI}k_{off-TnCl}[TnCl:Ca]$$

ADDITIONAL COMPONENTS OF ECC MODEL

Formulations for the Na^+ background current (I_{Nab}), Na^+/K^+ pump, I_{Kr}, the plateau K^+ current (I_{Kp}), time-independent K^+ current (I_{K1}), Ca^{2+}-activated Cl^- current (I_{ClCa}), Na^+/Ca^{2+} exchanger (I_{NCX}), sarcolemmal Ca^{2+} pump current (I_{pCa}), background Ca^{2+} current (I_{Cabk}), ionic buffering and diffusion are as in Shannon et al. (2004) (5).

SUPPLEMENTARY FIGURES

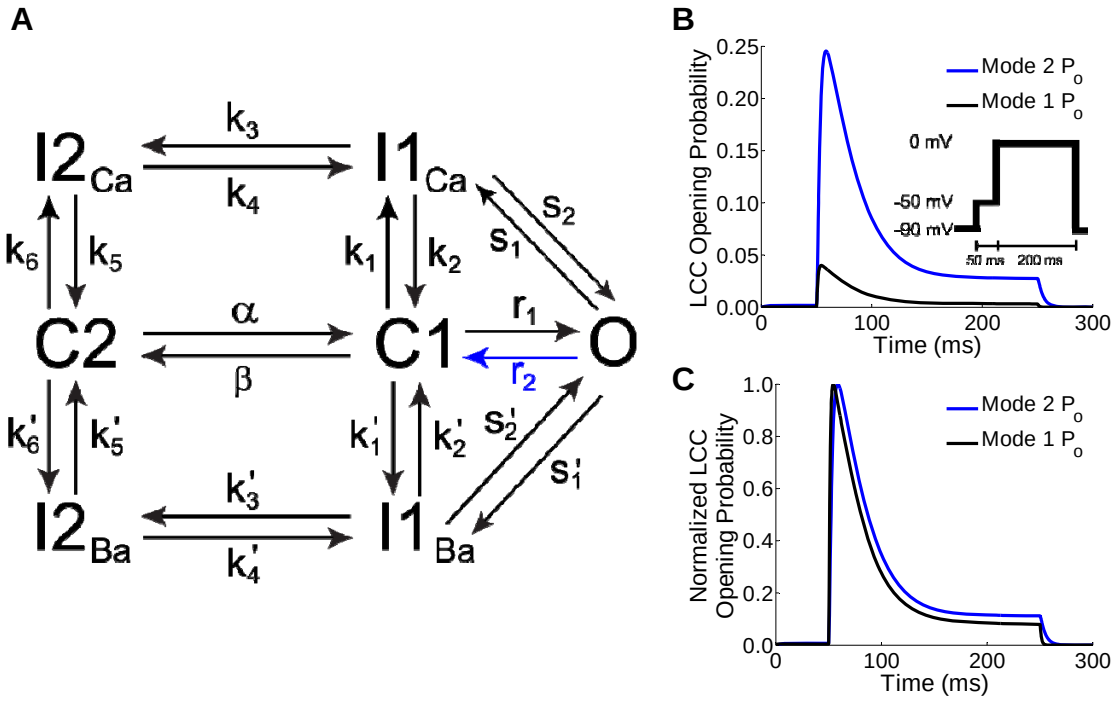

Figure S1. LCC Markov Model and LCC P_o. (**A**) Schematic of seven-state LCC Markov model. Parameter *r2* was modified to induce long-lasting openings for mode 2 channels. The fraction of channels in mode 1 or mode 2 in dyadic cleft or subsarcolemma ($junc_{m2}$ or sl_{m2}, respectively) is determined by CaMKII and PKA-dependent phosphorylation levels (see equations). (**B**) Dynamic changes in mode 1 (~0.05 peak P_o) and mode 2 (~0.25 peak P_o) LCC opening probabilities during voltage clamp (protocol shown in insert). (**C**) Normalization of traces shown in **B**, highlighting reduction in mode 2 channel inactivation rate. It is important to note that parameters *s2* and *s2'* shown in panel (**A**) are defined using the principal of detailed balance and are inversely proportional to the value of *r2*. Therefore, these parameters were also re-adjusted in cases where *r2* was altered.

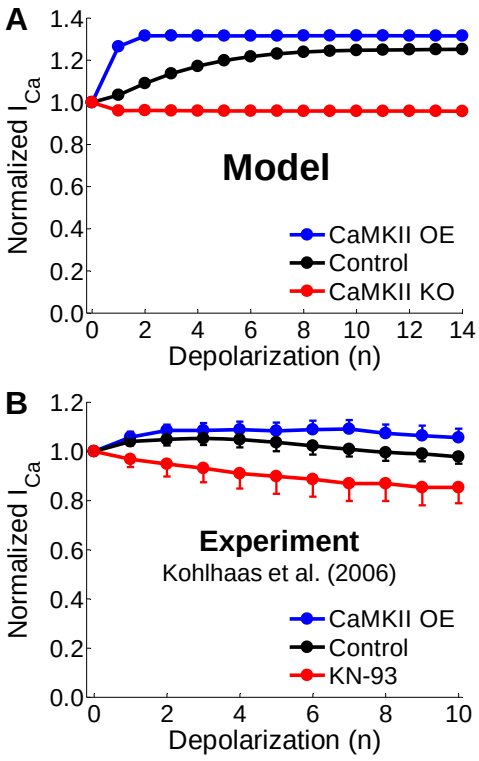

Figure S2. CaMKII is responsible for I_{Ca} facilitation (**A**) CaMKII induces a step-wise increase in I_{Ca} amplitude (facilitation) during 2.0 Hz voltage clamp stimulation from rest. CaMKII-OE enhances and hastens facilitation. During CaMKII-KO, facilitation is eliminated and successive currents are smaller than the first beat due to incomplete channel recovery from inactivation. (**B**) Experimental I_{Ca} facilitation from Kohlhaas et al. (1).

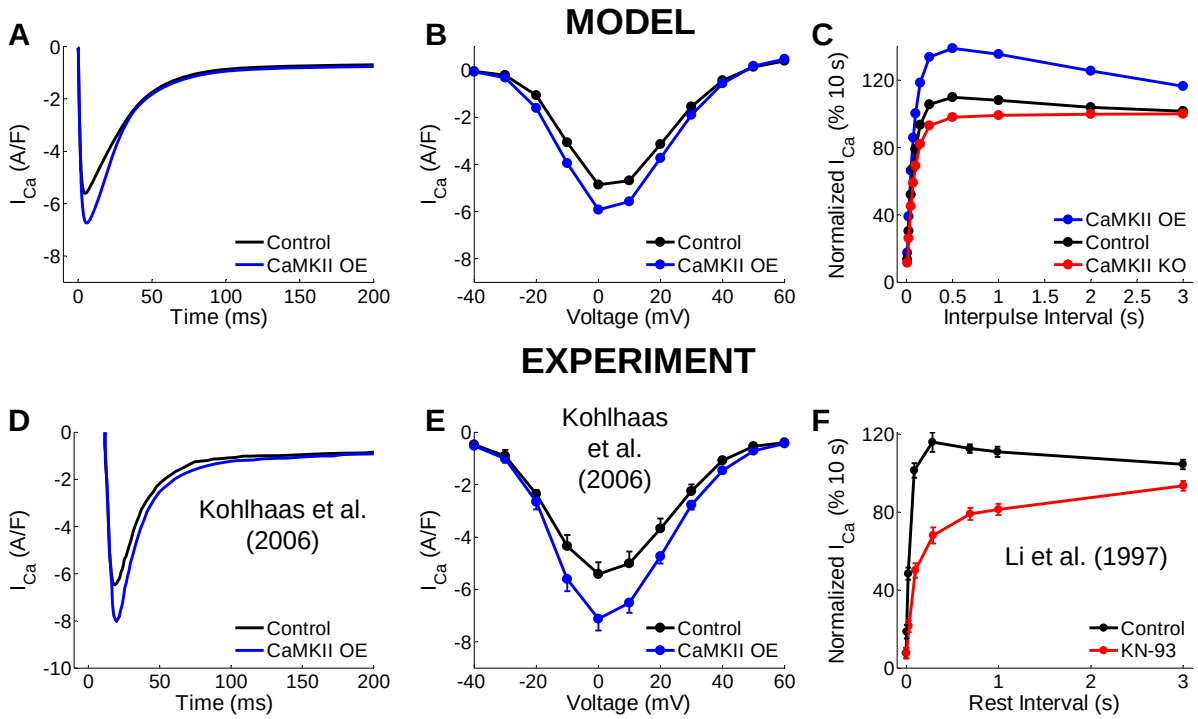

FIGURE S3. Additional properties of CaMKII-dependent I_{Ca} augmentation. (**A**) Comparison of steady-state macroscopic I_{Ca} kinetics with a 0 mV test potential during 0.5 Hz voltage clamp. Peak I_{Ca} increases from -5.6 to -6.74 A/F due to CaMKII-OE. (**B**) Current-voltage relationship shows increased peak I_{Ca} at a number of test potentials during 0.5 Hz voltage clamp with CaMKII-OE, though voltage dependence of peak I_{Ca} is unaltered. (**C**) CaMKII activity enhances apparent LCC recovery from inactivation. This effect is enhanced further during CaMKII-OE. (**D-F**) Sample experimental measures of CaMKII-dependent alterations to I_{Ca}: I_{Ca} kinetics (**D**) and I-V curves (**E**) from Kohlhaas et al. (1) and (**F**) recovery from inactivation from Li et al. (1997) (7).

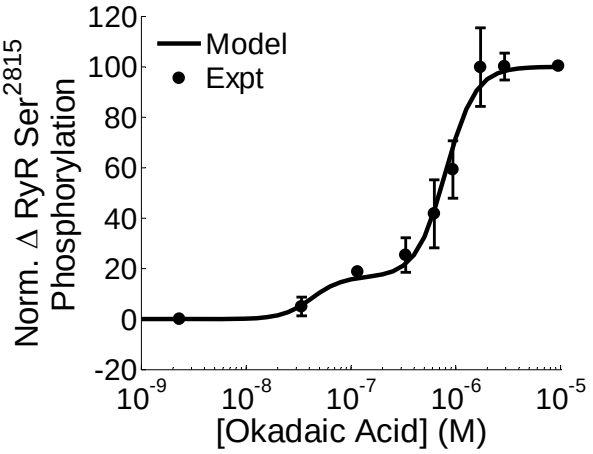

FIGURE S4. Biphasic Phosphatase action and basal phosphorylation at Ser^{2815} of RyR. PP1 and PP2A are both active at Ser^{2815} of RyRs, the main CaMKII phosphorylation site. Okadaic acid (OA) inhibits PP2A at low concentrations (IC_{50} ~2 nM) and PP1 at higher concentrations (IC_{50} ~270 nM). Model values are basal phosphorylation levels (i.e. no pacing, CaMKII activity < 1%) fit against experimental data points from Huke & Bers (1).

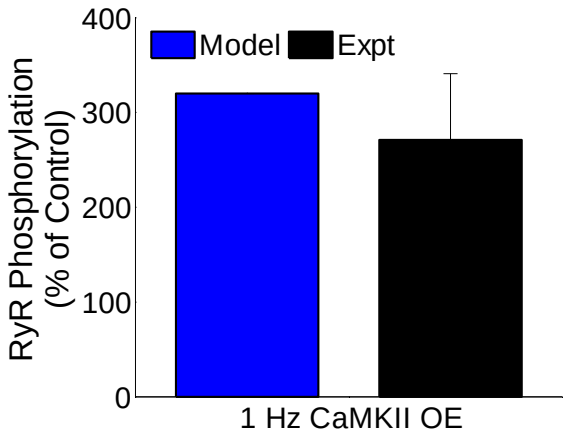

FIGURE S5. Quantitative increase in RyR Ser^{2815} phosphorylation due to CaMKII-OE. During 1 Hz pacing, Ser^{2815} phosphorylation increases ~3.3 times when CaMKII is overexpressed in the model. This quantitative increase is similar to that seen experimentally in rabbit myocytes (2.7 ± 0.7 times) overexpressing CaMKII (Kohlhaas et al. (2006) (1))

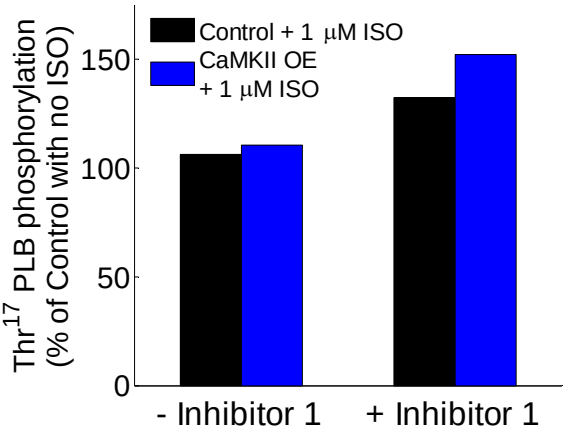

FIGURE S6. Inhibitor 1 enhances PLB Thr^{17} phosphorylation during β-adrenergic stimulation. During adrenergic stimulation, PKA activates inhibitor-1 which inhibits PP1 near PLB. In simulations with ISO, inclusion of this interaction resulted in an overall increase in PLB-Thr^{17} phosphorylation in both control and CaMKII-OE conditions.

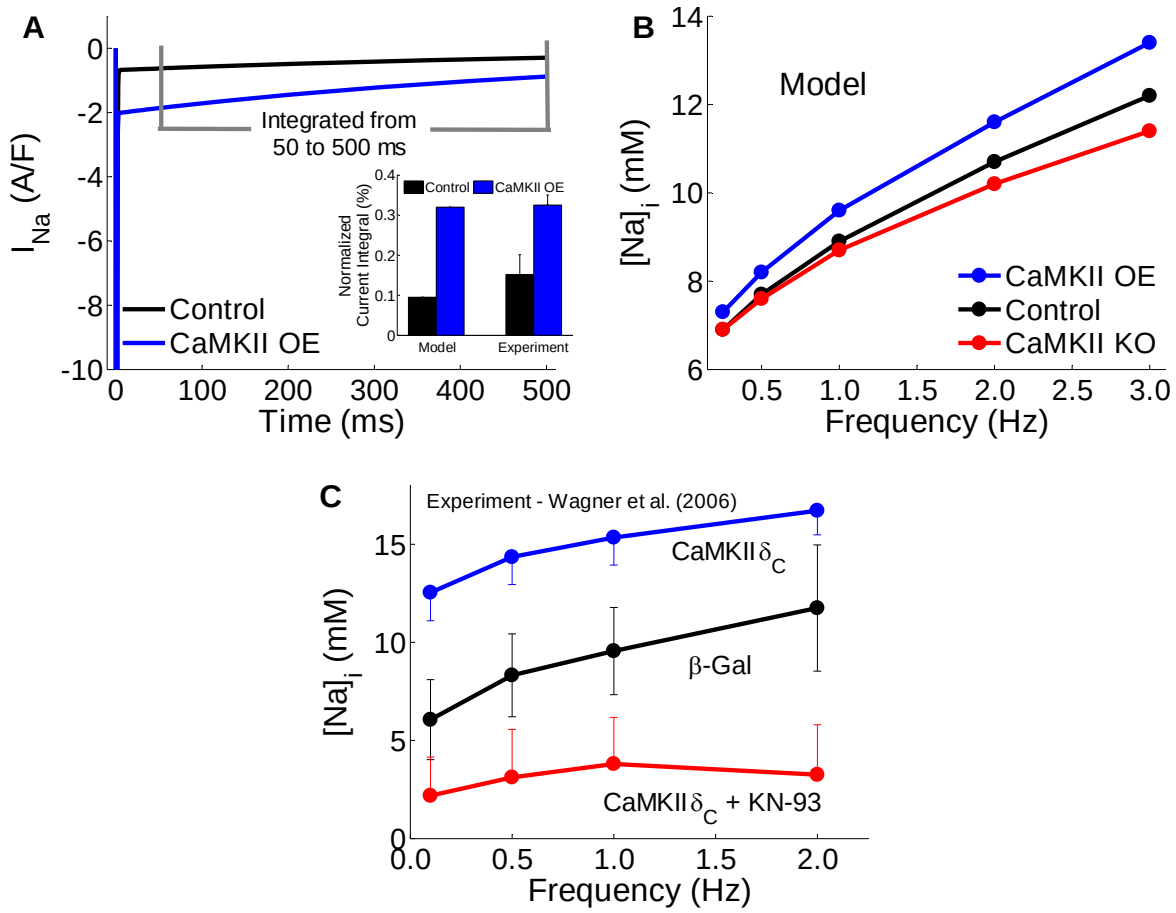

FIGURE S7. Alterations to $I_{Na,L}$, and $[Na]_i$ during CaMKII-OE. (**A**) Quantification of enhanced $I_{Na,L}$ during CaMKII OE simulations. Normalized current integrals were computed by integrating the late current from 50 to 500 ms and dividing the result by the integral if no inactivation had occurred (peak current x 450 ms). Insert shows comparison of model results to data from Wagner et al. (2006) (6). (**B**) Predicted $[Na]_i$ during control, CaMKII-OE, and CaMKII-KO simulations at various pacing frequencies. CaMKII-OE and KO slightly raised and lowered $[Na]_i$, respectively. (**C**) Reported $[Na]_i$ from CaMKII-OE (CaMKIIδ_C), control (β-Gal), and CaMKII inhibited (KN-93) rabbit myocytes from same study in (**A**). Model correctly predicts qualitative trends in $[Na]_i$ changes though absolute quantitative levels differ from experiments, suggesting additional mechanisms beyond $I_{Na(f,L)}$ interactions exist for CaMKII-dependent $[Na]_i$ regulation.

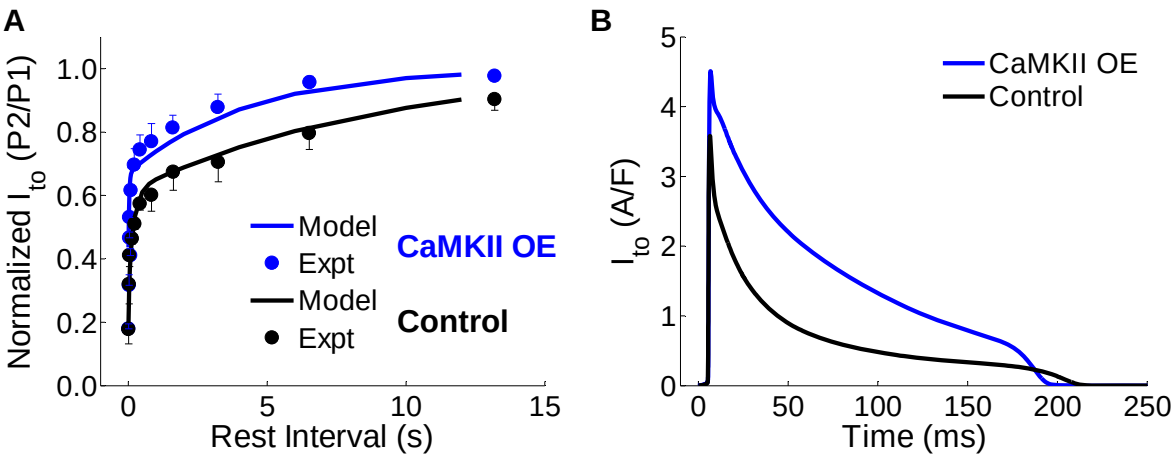

FIGURE S8. I_{to} Properties. (**A**) I_{to} recovery from inactivation hastens during CaMKII-OE simulations. Experimental data are from Wagner et al. (2009) (2). (**B**) Predicted I_{to} traces during 1 Hz pacing during control and CaMKII-OE simulations. Note that CaMKII increases current amplitude and causes total current to inactivate at an earlier time point (shortening APD).

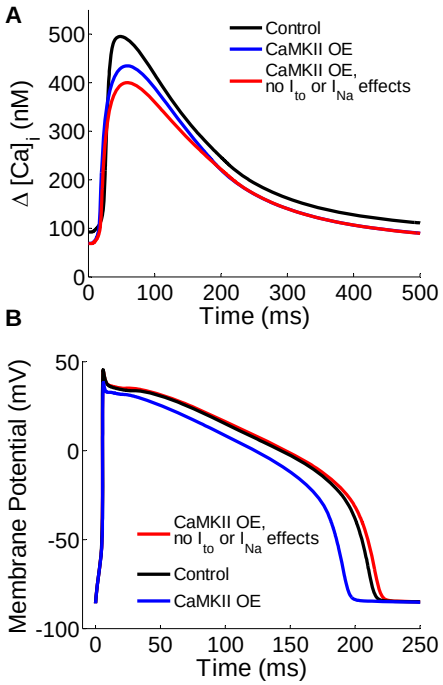

FIGURE S9. Net influence of I_{to} and I_{Na} effects on $[Ca^{2+}]_i$ and APD during CaMKII-OE. During 1 Hz pacing, CaMKII-OE slightly lowers $\Delta[Ca^{2+}]_i$ (from 402 to 365 nM) (**A**) and shortens APD (from 213 to 194 ms) (**B**). Simulations with CaMKII-OE but no I_{to} or I_{Na} effects predict slightly smaller $\Delta[Ca^{2+}]_i$ (331 nM) and slightly larger APD (218 ms) compared to control. Thus, alterations to I_{to} or I_{Na} during CaMKII-OE are essential for prediction of APD shortening but have modest effects on overall $[Ca^{2+}]_i$.

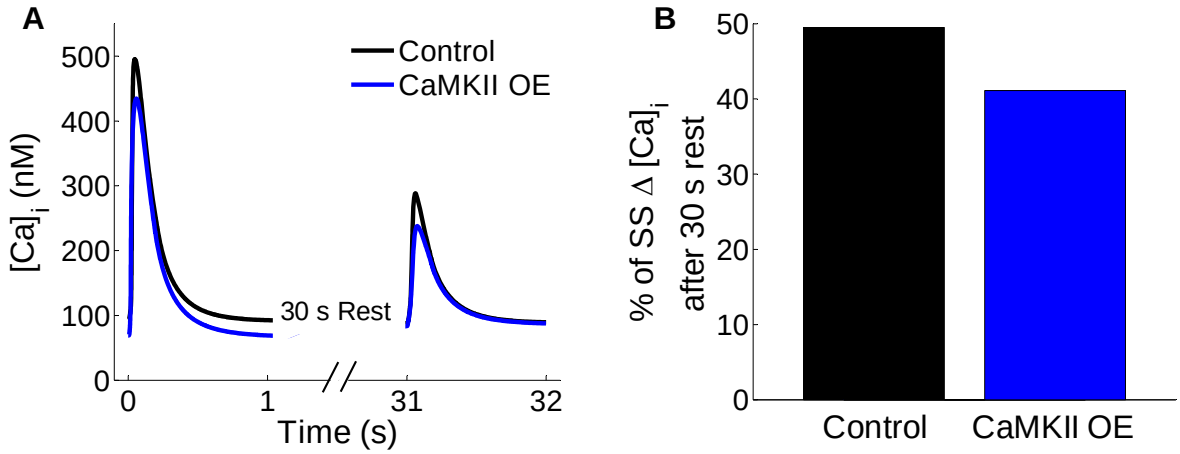

FIGURE S10. CaMKII-OE enhances post-rest decay of Ca^{2+} transient. (**A**) Post-rest (PR) decay was assessed by comparing pre-rest Ca^{2+} transient amplitudes (steady-state 1 Hz) to Ca^{2+} transients after 30 s rest. (**B**) Quantification of results in panel **A** demonstrates that CaMKII slightly enhances PR decay. This is consistent with experimental data from Kohlhaas *et al.* (4).

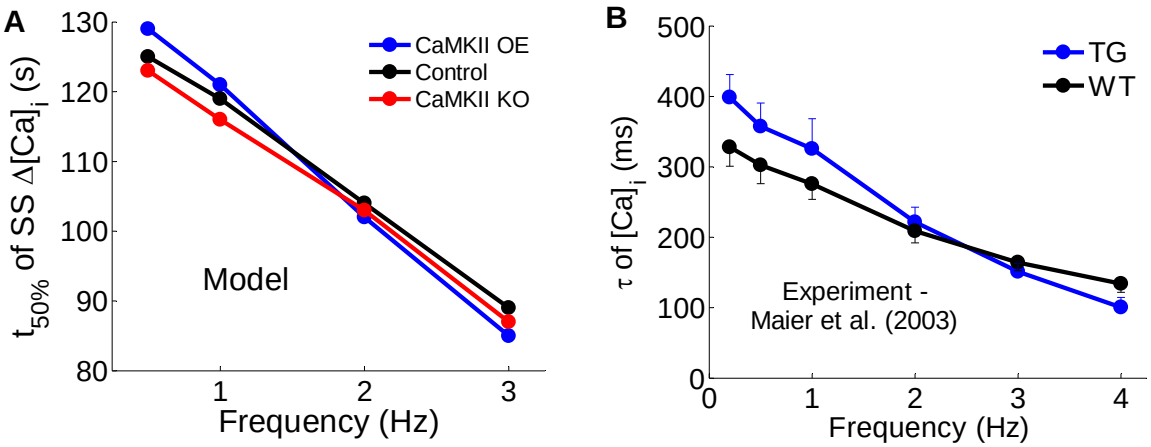

FIGURE S11. CaMKII-dependent regulation of steady-state frequency-dependent acceleration of relaxation (FDAR). The model exhibits normal FDAR, which is slightly CaMKII-dependent at steady state. CaMKII-OE makes the slope of steady-state FDAR more negative (consistent with experimental data show in (**B**) (3)), while the slope during CaMKII-KO is slightly less negative compared to control.

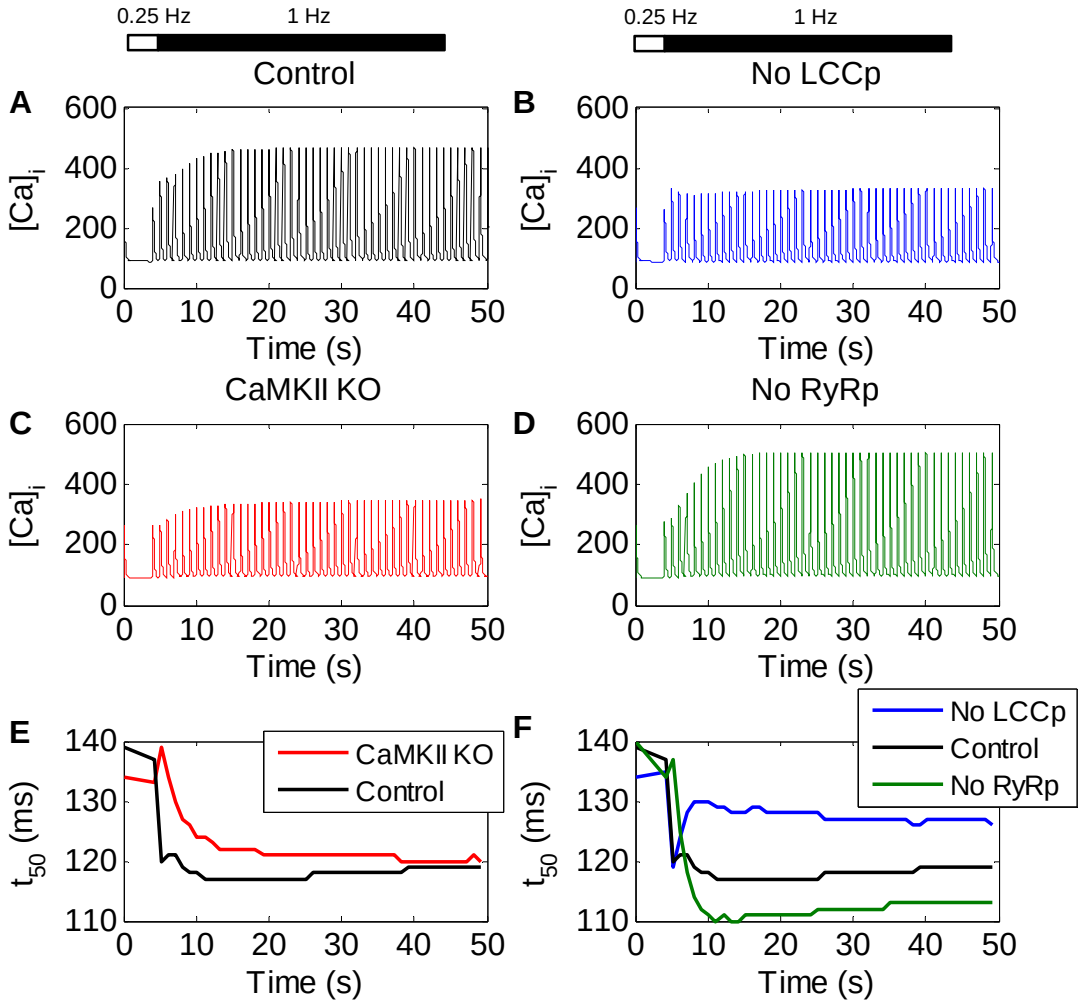

FIGURE S12. CaMKII enhances early FDAR via LCC phosphorylation. (**A-D**) $[Ca^{2+}]_i$ transients in response to an increase in pacing frequency. The model was paced to steady state at 0.25 Hz and switched to 1 Hz at 4 s. Panels **A** and **C** show time courses during control and CaMKII-KO simulations, respectively, while **B** and **D** show control simulations where CaMKII phosphorylation of LCCs and RyRs, respectively, were fixed at their diastolic 0.25 Hz levels (the model was otherwise like the control). (**E**) Time courses of t_{50} adaptation show rapid FDAR in control simulations that is slowed by CaMKII-KO. (**F**) Elimination of CaMKII-dependent LCC phosphorylation reduced early FDAR compared to control, while elimination of RyR phosphorylation enhanced early FDAR. This shows that CaMKII-LCC interactions are particularly important for the early phase of FDAR. Overall CaMKII-dependent FDAR is determined by a balance of LCC and RyR regulation.

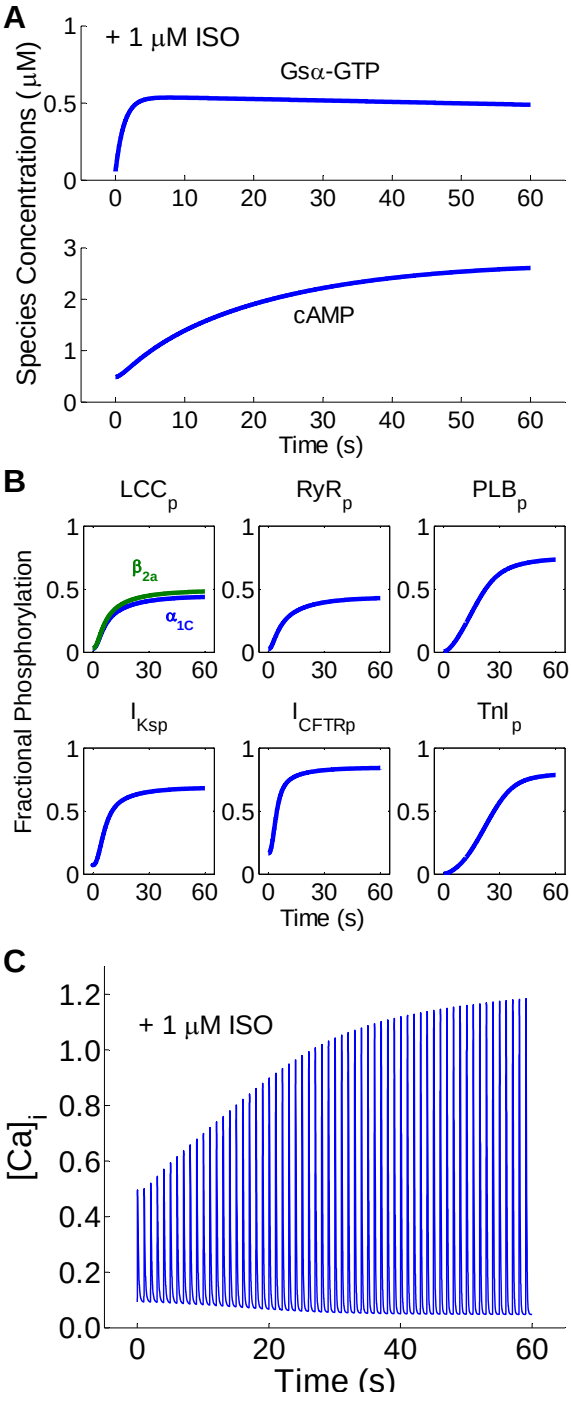

FIGURE S13. Time Course of β-adrenergic signaling. After reaching steady-state at 1 Hz pacing, 1 μM Isoproterenol was added to the model (at 0 s). Time courses for (**A**) Gsα –GTP, cAMP, (**B**) PKA substrates (LCC α_{1C} and β_{2a} subunits, RyR, PLB Ser^{16}, I_{Ks} channels, CFTR channels, and TnI) and (**C**) $[Ca]_i$ transients during ISO stimulation are shown.

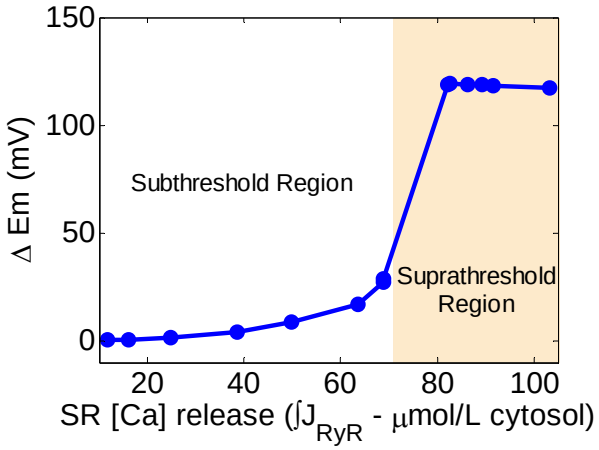

FIGURE S14. Quantification of SR Ca^{2+} release threshold for DADs. SR Ca^{2+} release following 2 Hz pacing (during CaMKII-OE with 1 μM ISO) producing sub (non-shaded) and supra threshold (shaded) DADs was quantified by integrating the total RyR release flux leading to the spontaneous depolarizations. Graded RyR release was obtained by scaling a RyR gating parameter k_{oSRCa} to varying degrees, similar to that caused by caffeine. The predicted SR Ca^{2+} release threshold for stimulation of a full DAD is ~70 μM, which is quantitatively consistent with the experimentally measured value of ~64 μM in Schlotthauer and Bers (2000) (4).

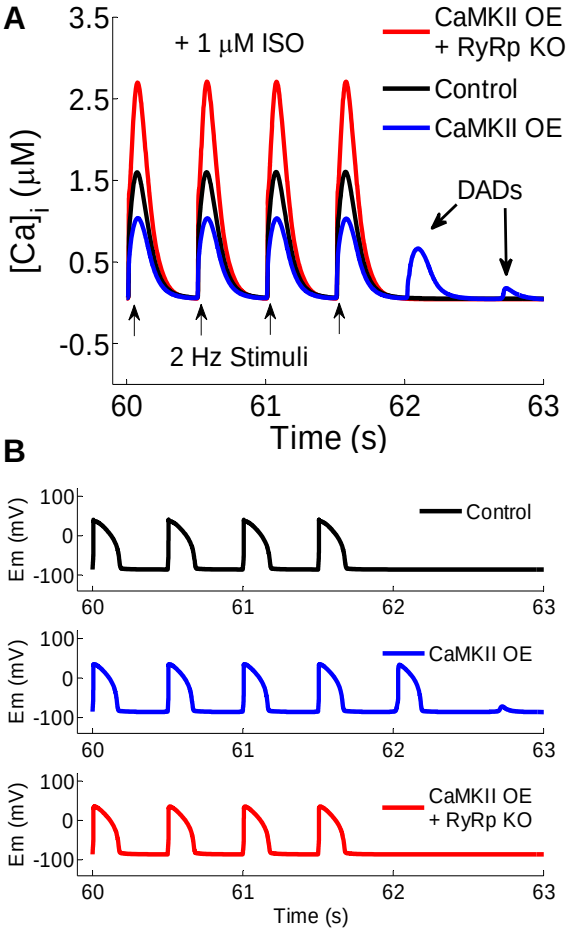

FIGURE S15. CaMKII-dependent RyR phosphorylation induces DAD formation. All simulations were performed in the presence of 1 μM ISO. (**A**) As in Fig. 6 of the main text, CaMKII OE + ISO produced DADs following stimulus removal at 2 Hz (blue trace), whereas control simulations did not (black trace). If RyR hyperphosphorylation by CaMKII is is restricted and all other targets retain functional regulation by CaMKII-OE, Ca^{2+} transients are dramatically enhanced, though DADs are eliminated. Similar results are shown in **B** when membrane potential is analyzed during the same simulations. These findings point to the key role of CaMKII-dependent RyR phosphorylation during DAD formation.

1. Kohlhaas, M., T. Zhang, T. Seidler, D. Zibrova, N. Dybkova, A. Steen, S. Wagner, L. Chen, J. H. Brown, D. M. Bers, and L. S. Maier. 2006. Increased sarcoplasmic reticulum calcium leak but unaltered contractility by acute CaMKII overexpression in isolated rabbit cardiac myocytes. Circ Res 98:235-244.
2. Wagner, S., E. Hacker, E. Grandi, S. L. Weber, N. Dybkova, S. Sossalla, T. Sowa, L. Fabritz, P. Kirchhof, D. M. Bers, and L. S. Maier. 2009. Ca/calmodulin kinase II differentially modulates potassium currents. Circ Arrhythm Electrophysiol 2:285-294.
3. Maier, L. S., T. Zhang, L. Chen, J. DeSantiago, J. H. Brown, and D. M. Bers. 2003. Transgenic CaMKIIdeltaC overexpression uniquely alters cardiac myocyte Ca2+ handling: reduced SR Ca2+ load and activated SR Ca2+ release. Circ Res 92:904-911.
4. Schlotthauer, K., and D. M. Bers. 2000. Sarcoplasmic reticulum Ca(2+) release causes myocyte depolarization. Underlying mechanism and threshold for triggered action potentials. Circ Res 87:774-780.
5. Shannon, T. R., F. Wang, J. Puglisi, C. Weber, and D. M. Bers. 2004. A mathematical treatment of integrated Ca dynamics within the ventricular myocyte. Biophys J 87:3351-3371.
6. Wagner, S., N. Dybkova, E. C. Rasenack, C. Jacobshagen, L. Fabritz, P. Kirchhof, S. K. Maier, T. Zhang, G. Hasenfuss, J. H. Brown, D. M. Bers, and L. S. Maier. 2006. Ca2+/calmodulin-dependent protein kinase II regulates cardiac Na+ channels. J Clin Invest 116:3127-3138.
7. Li, L., H. Satoh, K. S. Ginsburg, and D. M. Bers. 1997. The effect of Ca(2+)-calmodulin-dependent protein kinase II on cardiac excitation-contraction coupling in ferret ventricular myocytes. J Physiol 501 (Pt 1):17-31.
8. Bers, D. M. 2001. Excitation-Contraction Coupling and Cardiac Contractile Force. Kluwer Academic Publishers, Dordrecht.
9. Bers, D. M., and V. M. Stiffel. 1993. Ratio of ryanodine to dihydropyridine receptors in cardiac and skeletal muscle and implications for E-C coupling. Am J Physiol 264:C1587-1593.
10. Hove-Madsen, L., and D. M. Bers. 1993. Sarcoplasmic reticulum Ca2+ uptake and thapsigargin sensitivity in permeabilized rabbit and rat ventricular myocytes. Circ Res 73:820-828.
11. Marx, S. O., S. Reiken, Y. Hisamatsu, T. Jayaraman, D. Burkhoff, N. Rosemblit, and A. R. Marks. 2000. PKA phosphorylation dissociates FKBP12.6 from the calcium release channel (ryanodine receptor): defective regulation in failing hearts. Cell 101:365-376.
12. Saucerman, J. J., and D. M. Bers. 2008. Calmodulin mediates differential sensitivity of CaMKII and calcineurin to local Ca2+ in cardiac myocytes. Biophys J 95:4597-4612.
13. Gaertner, T. R., S. J. Kolodziej, D. Wang, R. Kobayashi, J. M. Koomen, J. K. Stoops, and M. N. Waxham. 2004. Comparative analyses of the three-dimensional structures and enzymatic properties of alpha, beta, gamma and delta isoforms of Ca2+-calmodulin-dependent protein kinase II. J Biol Chem 279:12484-12494.
14. Mayadevi, M., M. Praseeda, K. S. Kumar, and R. V. Omkumar. 2002. Sequence determinants on the NR2A and NR2B subunits of NMDA receptor responsible for specificity of phosphorylation by CaMKII. Biochim Biophys Acta 1598:40-45.
15. Huke, S., and D. M. Bers. 2007. Temporal dissociation of frequency-dependent acceleration of relaxation and protein phosphorylation by CaMKII. J Mol Cell Cardiol 42:590-599.

16. Bialojan, C., and A. Takai. 1988. Inhibitory effect of a marine-sponge toxin, okadaic acid, on protein phosphatases. Specificity and kinetics. Biochem J 256:283-290.
17. Takai, A., K. Tsuboi, M. Koyasu, and M. Isobe. 2000. Effects of modification of the hydrophobic C-1-C-16 segment of tautomycin on its affinity to type-1 and type-2A protein phosphatases. Biochem J 350 Pt 1:81-88.
18. Huke, S., and D. M. Bers. 2008. Ryanodine receptor phosphorylation at Serine 2030, 2808 and 2814 in rat cardiomyocytes. Biochem Biophys Res Commun 376:80-85.
19. Yamaguchi, H., G. Minopoli, O. N. Demidov, D. K. Chatterjee, C. W. Anderson, S. R. Durell, and E. Appella. 2005. Substrate specificity of the human protein phosphatase 2Cdelta, Wip1. Biochemistry 44:5285-5294.
20. Saucerman, J. J., S. N. Healy, M. E. Belik, J. L. Puglisi, and A. D. McCulloch. 2004. Proarrhythmic consequences of a KCNQ1 AKAP-binding domain mutation: computational models of whole cells and heterogeneous tissue. Circ Res 95:1216-1224.
21. Couchonnal, L. F., and M. E. Anderson. 2008. The role of calmodulin kinase II in myocardial physiology and disease. Physiology (Bethesda) 23:151-159.
22. Lee, T. S., R. Karl, S. Moosmang, P. Lenhardt, N. Klugbauer, F. Hofmann, T. Kleppisch, and A. Welling. 2006. Calmodulin kinase II is involved in voltage-dependent facilitation of the L-type Cav1.2 calcium channel: Identification of the phosphorylation sites. J Biol Chem 281:25560-25567.
23. Hudmon, A., H. Schulman, J. Kim, J. M. Maltez, R. W. Tsien, and G. S. Pitt. 2005. CaMKII tethers to L-type Ca2+ channels, establishing a local and dedicated integrator of Ca2+ signals for facilitation. J Cell Biol 171:537-547.
24. Grueter, C. E., S. A. Abiria, I. Dzhura, Y. Wu, A. J. Ham, P. J. Mohler, M. E. Anderson, and R. J. Colbran. 2006. L-type Ca2+ channel facilitation mediated by phosphorylation of the beta subunit by CaMKII. Mol Cell 23:641-650.
25. Ono, K., and H. A. Fozzard. 1993. Two phosphatase sites on the Ca2+ channel affecting different kinetic functions. J Physiol 470:73-84.
26. duBell, W. H., and T. B. Rogers. 2004. Protein phosphatase 1 and an opposing protein kinase regulate steady-state L-type Ca2+ current in mouse cardiac myocytes. J Physiol 556:79-93.
27. Dzhura, I., Y. Wu, R. J. Colbran, J. R. Balser, and M. E. Anderson. 2000. Calmodulin kinase determines calcium-dependent facilitation of L-type calcium channels. Nat Cell Biol 2:173-177.
28. Anderson, M. E., A. P. Braun, H. Schulman, and B. A. Premack. 1994. Multifunctional Ca2+/calmodulin-dependent protein kinase mediates Ca(2+)-induced enhancement of the L-type Ca2+ current in rabbit ventricular myocytes. Circ Res 75:854-861.
29. Yuan, W., and D. M. Bers. 1994. Ca-dependent facilitation of cardiac Ca current is due to Ca-calmodulin-dependent protein kinase. Am J Physiol 267:H982-993.
30. Hashambhoy, Y. L., R. L. Winslow, and J. L. Greenstein. 2009. CaMKII-induced shift in modal gating explains L-type Ca(2+) current facilitation: a modeling study. Biophys J 96:1770-1785.
31. Mahajan, A., Y. Shiferaw, D. Sato, A. Baher, R. Olcese, L. H. Xie, M. J. Yang, P. S. Chen, J. G. Restrepo, A. Karma, A. Garfinkel, Z. Qu, and J. N. Weiss. 2008. A rabbit ventricular action potential model replicating cardiac dynamics at rapid heart rates. Biophys J 94:392-410.

32. Tanskanen, A. J., J. L. Greenstein, B. O'Rourke, and R. L. Winslow. 2005. The role of stochastic and modal gating of cardiac L-type Ca2+ channels on early after-depolarizations. Biophys J 88:85-95.
33. Yue, D. T., S. Herzig, and E. Marban. 1990. Beta-adrenergic stimulation of calcium channels occurs by potentiation of high-activity gating modes. Proc Natl Acad Sci U S A 87:753-757.
34. Wehrens, X. H., S. E. Lehnart, S. R. Reiken, and A. R. Marks. 2004. Ca2+/calmodulin-dependent protein kinase II phosphorylation regulates the cardiac ryanodine receptor. Circ Res 94:e61-70.
35. Bers, D. M. 2006. Cardiac ryanodine receptor phosphorylation: target sites and functional consequences. Biochem J 396:e1-3.
36. Ferrero, P., M. Said, G. Sanchez, L. Vittone, C. Valverde, P. Donoso, A. Mattiazzi, and C. Mundina-Weilenmann. 2007. Ca2+/calmodulin kinase II increases ryanodine binding and Ca2+-induced sarcoplasmic reticulum Ca2+ release kinetics during beta-adrenergic stimulation. J Mol Cell Cardiol 43:281-291.
37. Rodriguez, P., M. S. Bhogal, and J. Colyer. 2003. Stoichiometric phosphorylation of cardiac ryanodine receptor on serine 2809 by calmodulin-dependent kinase II and protein kinase A. J Biol Chem 278:38593-38600.
38. Chelu, M. G., and X. H. Wehrens. 2007. Sarcoplasmic reticulum calcium leak and cardiac arrhythmias. Biochem Soc Trans 35:952-956.
39. Ai, X., J. W. Curran, T. R. Shannon, D. M. Bers, and S. M. Pogwizd. 2005. Ca2+/calmodulin-dependent protein kinase modulates cardiac ryanodine receptor phosphorylation and sarcoplasmic reticulum Ca2+ leak in heart failure. Circ Res 97:1314-1322.
40. Curran, J., M. J. Hinton, E. Rios, D. M. Bers, and T. R. Shannon. 2007. Beta-adrenergic enhancement of sarcoplasmic reticulum calcium leak in cardiac myocytes is mediated by calcium/calmodulin-dependent protein kinase. Circ Res 100:391-398.
41. Guo, T., T. Zhang, R. Mestril, and D. M. Bers. 2006. Ca2+/Calmodulin-dependent protein kinase II phosphorylation of ryanodine receptor does affect calcium sparks in mouse ventricular myocytes. Circ Res 99:398-406.
42. Wu, Y., R. J. Colbran, and M. E. Anderson. 2001. Calmodulin kinase is a molecular switch for cardiac excitation-contraction coupling. Proc Natl Acad Sci U S A 98:2877-2881.
43. Yang, D., W. Z. Zhu, B. Xiao, D. X. Brochet, S. R. Chen, E. G. Lakatta, R. P. Xiao, and H. Cheng. 2007. Ca2+/calmodulin kinase II-dependent phosphorylation of ryanodine receptors suppresses Ca2+ sparks and Ca2+ waves in cardiac myocytes. Circ Res 100:399-407.
44. Curran, J., K. H. Brown, D. J. Santiago, S. Pogwizd, D. M. Bers, and T. R. Shannon. 2010. Spontaneous Ca waves in ventricular myocytes from failing hearts depend on Ca(2+)-calmodulin-dependent protein kinase II. J Mol Cell Cardiol.
45. Picht, E., J. DeSantiago, S. Huke, M. A. Kaetzel, J. R. Dedman, and D. M. Bers. 2007. CaMKII inhibition targeted to the sarcoplasmic reticulum inhibits frequency-dependent acceleration of relaxation and Ca2+ current facilitation. J Mol Cell Cardiol 42:196-205.
46. Li, Y., E. G. Kranias, G. A. Mignery, and D. M. Bers. 2002. Protein kinase A phosphorylation of the ryanodine receptor does not affect calcium sparks in mouse ventricular myocytes. Circ Res 90:309-316.

47. Shannon, T. R., F. Wang, and D. M. Bers. 2005. Regulation of cardiac sarcoplasmic reticulum Ca release by luminal [Ca] and altered gating assessed with a mathematical model. Biophys J 89:4096-4110.
48. Simmerman, H. K., and L. R. Jones. 1998. Phospholamban: protein structure, mechanism of action, and role in cardiac function. Physiol Rev 78:921-947.
49. Colyer, J., and J. H. Wang. 1991. Dependence of cardiac sarcoplasmic reticulum calcium pump activity on the phosphorylation status of phospholamban. J Biol Chem 266:17486-17493.
50. Hagemann, D., M. Kuschel, T. Kuramochi, W. Zhu, H. Cheng, and R. P. Xiao. 2000. Frequency-encoding Thr17 phospholamban phosphorylation is independent of Ser16 phosphorylation in cardiac myocytes. J Biol Chem 275:22532-22536.
51. Zhao, W., Y. Uehara, G. Chu, Q. Song, J. Qian, K. Young, and E. G. Kranias. 2004. Threonine-17 phosphorylation of phospholamban: a key determinant of frequency-dependent increase of cardiac contractility. J Mol Cell Cardiol 37:607-612.
52. Kranias, E. G. 1985. Regulation of Ca2+ transport by cyclic 3',5'-AMP-dependent and calcium-calmodulin-dependent phosphorylation of cardiac sarcoplasmic reticulum. Biochim Biophys Acta 844:193-199.
53. Odermatt, A., K. Kurzydlowski, and D. H. MacLennan. 1996. The vmax of the Ca2+-ATPase of cardiac sarcoplasmic reticulum (SERCA2a) is not altered by Ca2+/calmodulin-dependent phosphorylation or by interaction with phospholamban. J Biol Chem 271:14206-14213.
54. Reddy, L. G., L. R. Jones, R. C. Pace, and D. L. Stokes. 1996. Purified, reconstituted cardiac Ca2+-ATPase is regulated by phospholamban but not by direct phosphorylation with Ca2+/calmodulin-dependent protein kinase. J Biol Chem 271:14964-14970.
55. Xu, A., and N. Narayanan. 1999. Ca2+/calmodulin-dependent phosphorylation of the Ca2+-ATPase, uncoupled from phospholamban, stimulates Ca2+-pumping in native cardiac sarcoplasmic reticulum. Biochem Biophys Res Commun 258:66-72.
56. Xu, A., T. Netticadan, D. L. Jones, and N. Narayanan. 1999. Serine phosphorylation of the sarcoplasmic reticulum Ca(2+)-ATPase in the intact beating rabbit heart. Biochem Biophys Res Commun 264:241-246.
57. Valverde, C. A., C. Mundina-Weilenmann, M. Said, P. Ferrero, L. Vittone, M. Salas, J. Palomeque, M. V. Petroff, and A. Mattiazzi. 2005. Frequency-dependent acceleration of relaxation in mammalian heart: a property not relying on phospholamban and SERCA2a phosphorylation. J Physiol 562:801-813.
58. Iyer, R. B., S. B. Koritz, and M. A. Kirchberger. 1988. A regulation of the level of phosphorylated phospholamban by inhibitor-1 in rat heart preparations in vitro. Mol Cell Endocrinol 55:1-6.
59. Neumann, J., R. C. Gupta, W. Schmitz, H. Scholz, A. C. Nairn, and A. M. Watanabe. 1991. Evidence for isoproterenol-induced phosphorylation of phosphatase inhibitor-1 in the intact heart. Circ Res 69:1450-1457.
60. Chu, G., J. W. Lester, K. B. Young, W. Luo, J. Zhai, and E. G. Kranias. 2000. A single site (Ser16) phosphorylation in phospholamban is sufficient in mediating its maximal cardiac responses to beta -agonists. J Biol Chem 275:38938-38943.
61. Hund, T. J., K. F. Decker, E. Kanter, P. J. Mohler, P. A. Boyden, R. B. Schuessler, K. A. Yamada, and Y. Rudy. 2008. Role of activated CaMKII in abnormal calcium homeostasis

and I(Na) remodeling after myocardial infarction: insights from mathematical modeling. J Mol Cell Cardiol 45:420-428.
62. Grandi, E., J. L. Puglisi, S. Wagner, L. S. Maier, S. Severi, and D. M. Bers. 2007. Simulation of Ca-calmodulin-dependent protein kinase II on rabbit ventricular myocyte ion currents and action potentials. Biophys J 93:3835-3847.
63. Harvey, R. D., and J. R. Hume. 1989. Isoproterenol activates a chloride current, not the transient outward current, in rabbit ventricular myocytes. Am J Physiol 257:C1177-1181.
64. Ackerman, M. J., and D. E. Clapham. Cardiac chloride channels. Trends Cardiovasc Med 3:23-28.
65. Hart, P., J. D. Warth, P. C. Levesque, M. L. Collier, Y. Geary, B. Horowitz, and J. R. Hume. 1996. Cystic fibrosis gene encodes a cAMP-dependent chloride channel in heart. Proc Natl Acad Sci U S A 93:6343-6348.
66. Kockskamper, J., K. Sendhoff, S. Erlenkamp, F. Bordusa, V. Cerovsky, and H. G. Glitsch. 2001. Differences in the protein-kinase-A-dependent regulation of CFTR Cl-channels and Na+-K+ pumps in guinea-pig ventricular myocytes. Pflugers Arch 441:807-815.
67. Saucerman, J. J., L. L. Brunton, A. P. Michailova, and A. D. McCulloch. 2003. Modeling beta-adrenergic control of cardiac myocyte contractility in silico. J Biol Chem 278:47997-48003.
68. Saucerman, J. J., and A. D. McCulloch. 2004. Mechanistic systems models of cell signaling networks: a case study of myocyte adrenergic regulation. Prog Biophys Mol Biol 85:261-278.